Estd : 1995

GOVERNMENT DEGREE COLLEGE

KARVETINAGARAM, Chittoor Dt. - 517582

Accredited by NAAC 'B' Grade

ISO Certified 9001 : 2015

Website : www.gdcknagaram.edu.in E-Mail : knagaram.jkc@gmail.com

Dr. S. Vijayulu Reddy, *M.Com., M.Phil., Ph.D.,*

Principal

Date : 10-03-2023.

3.3.1 Number of research papers published per teacher in the Journals notified on UGC care list during the last five years

3.3.1.1. **Number of research papers in the Journals notified on UGC CARE list year wise during the last five years**

HEI Input :

2021-22	2020-21	2019-20	2018-19	2017-18
7	1	0	1	0

DVV suggested Input :

2021-22	2020-21	2019-20	2018-19	2017-18
1	1	0	1	0

CLARIFICATION:

As per DVV suggested,

Change Input :

2021-22	2020-21	2019-20	2018-19	2017-18
1	1	0	1	0

- Provided the link in the data template is not in Google drive format.
- Provided the revised data as per DVV suggestions.
- Provided that the list of publications submitted are in UGC care list.

PRINCIPAL
Govt. Degree College
KARVETINAGAR - 517582
Chittoor Dt. A.P.

GOVERNMENT DEGREE COLLEGE
KARVETINAGARAM, CHITTOOR (DT), A.P.

Criteria-3

3.3.1: ***Number of research papers published per teacher in the Journals notified on UGC care list during the last five years***

2017-18 to 2021-22

Estd : 1995

GOVERNMENT DEGREE COLLEGE

KARVETINAGARAM, Chittoor Dt. - 517582

Accredited by NAAC 'B' Grade

ISO Certified 9001 : 2015

Website : www.gdcknagaram.edu.in E-Mail : knagaram.jkc@gmail.com

Dr. S. Vijayulu Reddy, *M.Com., M.Phil., Ph.D.,*
Principal

Date: 10-03-2023

TO WHOMSOEVER IT MAY CONCERN

This is to certify that the number of research papers published per teacher in the journals notified on UGC care list during last five years.

The details are given below:

Year	2021-22	2020-21	2019-20	2018-19	2017-18
No. of Papers	1	1	0	1	0

PRINCIPAL
Govt. Degree College
KARVETINAGAR - 517582
Chittoor Dt. A.P.

Scanned with CamScanner

3.3.1 Number of research papers published per teacher in the Journals notified on UGC website during the last five years

Title of paper	Name of the author/s	Department of the teacher	Name of journal	Year of publication	ISSN number	Link to the recognition in UGC enlistment of the Journal /Digital Object Identifier (doi) number		
						Link to website of the Journal	Link to article / paper / abstract of the article	Is it listed in UGC Care list
Impacts of MHD boundary layer flow and melting heat transfer with chemical reaction and radiation	**Dr. A. Subbarao, Dr.K. Srinivasa Rao, Dr. K. Naresh Kumar, P. Rajani Kumari**	**Physics**	**Journal of Applied Science and Computations**	**Jul.2021**	**0022-1945**	http://j-asc.com/	https://drive.google.com/file/d/1ICr13xs3t7n31FMcUctXHvoUXkm2LoGp/view	Yes
Tourism in India Impact & Initiatives	**Dr. S. Vijayulu Reddy & P. Revathi Reddy**	**Commerce**	**International Journal of Multidisciplinary Educational Research**	**Nov.2020**	**2277-7881**	http://www.ijmer.in/	http://s3-ap-southeast-1.amazonaws.com/ijmer/pdf/volume9/volume9-issue11(6)-2020.pdf	Yes
Volumetric, acoustic and spectroscopic approaches to understand the molecular interactions between 1-butyl-3-methylimidazolium hexafluorophosphate and N-vinyl-2-pyrrolidinone	**P. Suneetha, Dr.D.Ramachandran, T.S. Krishna, M. Gowrisankar & M. Srinivasa Reddy**	**Chemistry**	**Journal of Thermal Analysis and Calorimetry**	**Jun.2018**	**10973-018-7427-0**	https://www.springer.com/journal/10973	https://link.springer.com/article/10.1007/s10973-018-7427-0	Yes

PRINCIPAL
Govt. Degree College
KARVETINAGAR - 517582
Chittoor Dt. A.P.

Scanned with CamScanner

Impacts of MHD boundary layer flow and melting heat transfer with chemical reaction and radiation

Dr A Subba Rao[1], Dr K Srinivasa Rao[2], Dr K Naresh Kumar[3], P Rajani Kumari [4]

[1]Department of Physics, S.S. & N. College, Narasaraopet- 522601, A.P. (INDIA)
[2]Department of Physics, Bapatla College of Arts & Science, Bapatla -522101, A.P. (INDIA)
[3]Department of Physics, V.R.S & Y.R.N College, Chirala -523155, A.P. (INDIA)
[4]Department of Chemistry, S.S. & N. College, Narasaraopet- 522601, A.P. (INDIA)
[*]E-mail: anumula.subbarao@gmail.com

Abstract

The present investigation deals with the study of the effects of chemical reaction and thermal radiation on the steady MHD boundary layer flow and heat transfer melting of Williamson nanofluid embedded in porous medium over a horizontal linearly stretching sheet under the influence of heat source and viscous dissipation. The governing momentum boundary layer and thermal boundary layer equations with the boundary conditions are transformed into a system of nonlinear ordinary differential equations which are then solved numerically by using the Runge–Kutta–Fehlberg method. Numerical results for the dimensionless velocity, temperature and concentration profiles as well as for the skin friction factor, Nusselt number and Sherwood number are elucidated for different values of the pertinent parameters. Comparison with existing literature is shown and it found to be in good agreement.

Keywords: ***Heat transfer melting parameter; MHD; Boundary layer; Chemical reaction; Viscous dissipation; nanofluids.***

Introduction

Nanofluids are attracting a great deal of interest due to their enormous potential with respect to enhanced heat transfer. The term “nanofluid” describes a liquid suspension composed of tiny particles of diameter less than 100 nm. It defines an important class of fluids, which has a distinctive ability to improve the thermal properties of fluids. The effective thermal conductivity

of the base fluid is appreciably enhanced as a consequence of the addition of small amount of nanoparticles according to the experimental verification by Choi [1]. Kleinstreuer and Feng [2] derived the experimental and theoretical studies of nanofluid thermal conductivity enhancement. The comparison of nanofluid thermal conductivity and heat transfer enhancements was studied by Yu et al. [3]. Eapen et al. [4] derived the classical nature of thermal conduction in nanofluids. Chitra and Sendhilnathan [5] investigated on the thermal studies of nanofluids related to their applications. The effects of Brownian motion and thermophoresis added into nanofluid model was first derived by Buongiorno [6].

Magneto hydrodynamic boundary-layer flow of nanofluid and heat transfer has received a lot of attention in the field of several industrial, scientific, and engineering applications in recent years. Mabood et al. [8] proposed a numerical study on MHD boundary layer flow of Nano fluids over a nonlinear stretching sheet with heat transfer effect. Analytical solution of free convective flow of a nanofluid over a stretching sheet in the presence of magnetic field was carried out by Hamad [9]. Ibrahim et al. [10] studied the MHD stagnation point flow and heat transfer due to nanofluid towards a stretching sheet. MHD boundary layer flow of a nanofluid past a wedge was illustrated by Srinivasacharya et al. [11].

Motivated by some of the researchers mentioned above and its applications in various fields of science and technology, it is of interest to discuss and analyze the thermal radiation and chemical reaction effects on the MHD boundary layer flow and melting heat transfer of Williamson nanofluid in a porous medium under the influence of viscous dissipation and heat generation. In the present study, the governing equations are solved numerically by Runge-Kutta –Fehlberg 45 method along with shooting technique.

Mathematical formulation

A steady two-dimensional flow of viscous incompressible Williamson nan fluid over a stretching surface in a porous medium is considered. The plate is stretched along x-axis with a velocity *ax*, where $a > 0$ is stretching parameter. U_w, T_w and C_w are the velocity, temperature and nanoparticle concentration near surface. Let the temperature of the melting surface as T_m, and temperature in the free-stream condition as T_∞, where $T_\infty > T_m$. The viscous dissipation and heat source or absorption are added into the flow. For the present paper, the basic equations of

conservation of mass, momentum, energy and concentration for steady flow of nanofluid can be represented as:

$$\frac{\partial u}{\partial x}+\frac{\partial v}{\partial y}=0 \tag{1}$$

$$u\frac{\partial u}{\partial x}+v\frac{\partial u}{\partial y}=\nu\frac{\partial^2 u}{\partial y^2}+\sqrt{2}\nu\Gamma\frac{\partial u}{\partial y}\frac{\partial^2 u}{\partial y^2}-\frac{\sigma B_0^2}{\rho}u-\frac{\nu}{k'}u \tag{2}$$

$$u\frac{\partial T}{\partial x}+v\frac{\partial T}{\partial y}=\alpha_m\frac{\partial^2 T}{\partial y^2}+\tau\left[D_B\frac{\partial C}{\partial y}\frac{\partial T}{\partial y}+\frac{D_T}{T_\infty}\left(\frac{\partial T}{\partial y}\right)^2\right]-\frac{1}{(\rho c)_f}\frac{\partial q_r}{\partial y}+ \tag{3}$$

$$u\frac{\partial C}{\partial x}+v\frac{\partial C}{\partial y}=D_B\frac{\partial^2 C}{\partial y^2}+\frac{D_T}{T_\infty}\frac{\partial^2 T}{\partial y^2}-k_0 C \tag{4}$$

The corresponding boundary conditions are:

$$u=U_w(x)=ax, \qquad T=T_m,\ k\left(\frac{\partial T}{\partial y}\right)=\rho\left(\lambda+c_s\left(T_m-T_s\right)\right)v(x,0),\ C=C_w \ \text{at}\ y=0,$$

$$u=0,\ T\to T_\infty \qquad C\to C_\infty \quad \text{as} \quad y\to\infty \tag{5}$$

where u, v are the velocity components along the x and y axes, ρ is density of the nanofluid, ν is the kinematic viscosity, B_o is the induced magnetic field, k' is the permeability of porous medium, τ is the ratio between the effective heat capacity of the nanoparticle material and the fluid, Γ is time constant, T is the nanofluid temperature, C is the volumetric volume expansion coefficient, T_w is the temperature of the nanofluid near wall, T_∞ is the free stream temperature of the nanofluid, k is the thermal conductivity, T_m is the melting temperature, T_s is the temperature of solid surface, λ is the latent heat of the fluid, c_s is the heat capacity of solid surface, U_w is the stretching sheet velocity, a is the stretching rate being a positive constant, c_p is the specific heat at constant pressure, q_r is the radiative heat flux, Q' is the heat generation coefficient, D_B is the

Brownian diffusion coefficient, D_T is the thermophoresis diffusion coefficient, k_o is the chemical reaction coefficient.

Using Rosseland approximation for radiation, the radiative heat flux is simplified as,

$$q_r = -\frac{4\sigma^*}{3k^*}\frac{\partial T^4}{\partial y} \tag{6}$$

where σ^* is the Stephen Boltzmann constant and k^* is the mean absorption coefficient.

It should be noted that by using the Rosseland approximation, the present analysis is limited to optically thick fluids. If the temperature differences within the flow are sufficiently small, then equation (6) can be linearized by expanding T^4 into the Taylor series about T_∞, which after neglecting higher order terms takes the form

$$T^4 \cong 4T_\infty^3 T - 3T_\infty^4 \tag{7}$$

Substituting (6) and (7) in (3), we have

$$u\frac{\partial T}{\partial x} + v\frac{\partial T}{\partial y} = \alpha_m \frac{\partial^2 T}{\partial y^2} + \tau\left[D_B\left(\frac{\partial C}{\partial y}\frac{\partial T}{\partial y}\right) + \frac{D_T}{T_\infty}\left(\frac{\partial T}{\partial y}\right)^2\right] + \frac{16\sigma^*}{3k^*}\frac{T_\infty^3}{(\rho c)_f}\frac{\partial^2 T}{\partial y^2} + \frac{\upsilon}{c}\left(\frac{\partial u}{\partial y}\right)^2 + \frac{Q'}{(\rho c)_f}(T - T_\infty) \tag{8}$$

The governing equations can be reduced to ordinary differential equations, using the following similarity transformation,

$$\psi = (a\nu)^{\frac{1}{2}} x f(\eta), \qquad \eta = \left(\frac{a}{\nu}\right)^{\frac{1}{2}} y, \quad \theta(\eta) = \frac{T - T_m}{T_\infty - T_m}, \qquad \phi(\eta) = \frac{C - C_w}{C_\infty - C_w}, \tag{9}$$

The stream function ψ is defined such that $u = \frac{\partial \psi}{\partial y}$ and $v = -\frac{\partial \psi}{\partial x}$

With the help of transformations, equation (1) is clearly satisfied, and equations (2), (4) and (8) along with boundary condition (5) take into the following form

$$f'''(\eta)+f(\eta)f''(\eta)-\left(f'(\eta)\right)^2+\lambda f''(\eta)f'''(\eta)-(M+K)f'=0 \tag{10}$$

$$\left(1+\frac{4}{3}R\right)\theta''(\eta)+\Pr f(\eta)\theta'(\eta)+\Pr Nb\theta'(\eta)\phi'(\eta)+\Pr Nt\left(\theta'(\eta)\right)^2+\Pr Ecf''^2+\Pr Q\theta(\eta)=0 \tag{11}$$

$$\phi''(\eta)+Lef(\eta)\phi'(\eta)+\frac{Nt}{Nb}\theta''(\eta)-\gamma\phi(\eta)=0 \tag{12}$$

The corresponding boundary conditions will take the form

$$f'(0)=1.0,\ \Pr f(0)+Me\theta'(0)=0,\ \theta(0)=0,\ \phi(0)=0,$$

$$f'(\infty)=0.0,\quad \theta(\infty)=1.0,\quad \phi(\infty)=1.0. \tag{13}$$

$M=\frac{\sigma B_0^2}{\rho a}$ is the magnetic parameter; $K=\frac{\nu}{k'a}$ is the permeability parameter; $\lambda=\Gamma x\left(\frac{2a^3}{\nu}\right)^{\frac{1}{2}}$ is the non-Newtonian Williamson parameter; $\alpha_m=\frac{k}{(\rho c)_f}$ is thermal diffusivity of nanofluid;

$\Pr=\frac{\nu}{\alpha_m}$ is Prandtl number; $\tau=\frac{(\rho c)_p}{(\rho c)_f}$ is ratio between the effective heat capacity of the nanoparticle material and the fluid; $Q=\frac{Q'}{a\rho c_p}$ is the heat generation parameter; $Ec=\frac{U_w^2}{c_p(T_\infty-T_m)}$ is the Eckert number; $R=\frac{4\sigma^* T_\infty^3}{kk^*}$ is the radiation parameter; $Nb=\frac{\tau D_B(C_\infty-C_w)}{\nu}$ is Brownian motion parameter; $Nt=\frac{\tau D_T(T_\infty-T_m)}{\nu T_\infty}$ is the themophoresis parameter; $Le=\frac{\nu}{D_B}$ is the Lewis number; $Kr=\frac{k_o U_w(C_\infty-C_w)}{\nu}$ is the chemical reaction parameter; $Me=\frac{c_f(T_\infty-T_m)}{\lambda+c_s(T_m-T_s)}$ is the dimensionless parameter;

The physical quantities of interest like skin-friction coefficient (C_f), local Nusselt number (Nu_x) and local Sherwood number (Sh_x) are defined as

$$C_f = \frac{\tau_w}{\rho U_w^2}, \quad Nu_x = \frac{xq_w}{k(T_\infty - T_m)} \text{ and } \quad Sh_x = \frac{xq_m}{D_B(C_\infty - C_m)} \tag{14}$$

where the shear stress (τ_w), surface heat flux (q_w) and surface mass flux (q_m) are given by

$$\tau_w = \mu\left[\frac{\partial u}{\partial y} + \frac{\Gamma}{\sqrt{2}}\left(\frac{\partial u}{\partial y}\right)^2\right], \quad q_w = -k\frac{\partial T}{\partial y}, \quad q_m = -D_B\frac{\partial C}{\partial y} \quad \text{at } y = 0$$

Using the non-dimensional variables, we obtain

$$C_f\left(\mathrm{Re}_x\right)^{-\frac{1}{2}} = f''(0) + \frac{\lambda}{2}f''(0)^2, \quad Nu_x\left(\mathrm{Re}_x\right)^{-\frac{1}{2}} = -\theta'(0) \text{ and } Sh_x\left(\mathrm{Re}_x\right)^{-\frac{1}{2}} = -\phi'(0)$$

where $\mathrm{Re}_x = \frac{xU_w(x)}{\nu}$ is the local Reynold's number.

Results and discussion

We reveal the results to keep up the influence of several non-dimensional parameters such as melting parameter, magnetic field parameter and other parameters on the three usual profiles (velocity, temperature and concentration). Also we examined the same parameters on skin friction coefficient, heat transfer rate and mass transfer rate with the aid of table. In this paper, we have chosen the non-dimensional parameter values as *M = 0.5, Me = 0.5, K = 0.5,* $\lambda = 0.2$, *R = 0.01, Pr = 2, Nb = 0.1, Nt = 0.1, Le = 10.0, Ec = 0.01, Q = 0.01 and Kr = 0.05.* These values are maintained as invariable in this study unless the varied parameters as depicted in the figures.

In figures 1- 20, we presented the highlights of the effects of the governing parameters on the nanofluid velocity, temperature and concentration profiles on the plate surface.

Figures 1 -3 depict the effects of magnetic field parameter on velocity, temperature and concentration profiles, respectively. it is observed that all the fields are decreases significantly with increasing magnetic field parameter. This would happen because the application of a transverse magnetic field sets up the Lorentz force, which retards the nanofluid velocity.

The effects of different values of permeability parameter on velocity, temperature and concentration fields are presented in Figs. 4 – 6. It is obvious that the presence of porous medium causes higher restriction to the fluid flow, which in turn slows its motion. Therefore, with increasing permeability parameter, the resistance to the fluid motion increases and hence velocity decreases. Temperature and concentration fields are also decreases with increasing permeability parameter. Figs. 7 – 8 explain the effect of melting parameter on velocity, temperature and concentration fields. It is noticed that for increasing values of melting parameter values, the velocity and the boundary layer thickness increase and decrease the temperature and concentration profiles. Reason for this behavior is an increase in melting parameter will increase the intensity of melting, which acts as blowing boundary condition at the surface and hence tends to thicken the boundary layer.

The variation of velocity, temperature and concentration distributions with non-Newtonian Williamson parameter is studied in Figs. 10 – 12. From these figures we observed that the nanofluid velocity, temperature and concentration decreases with increase in non-Newtonian Williamson parameter.

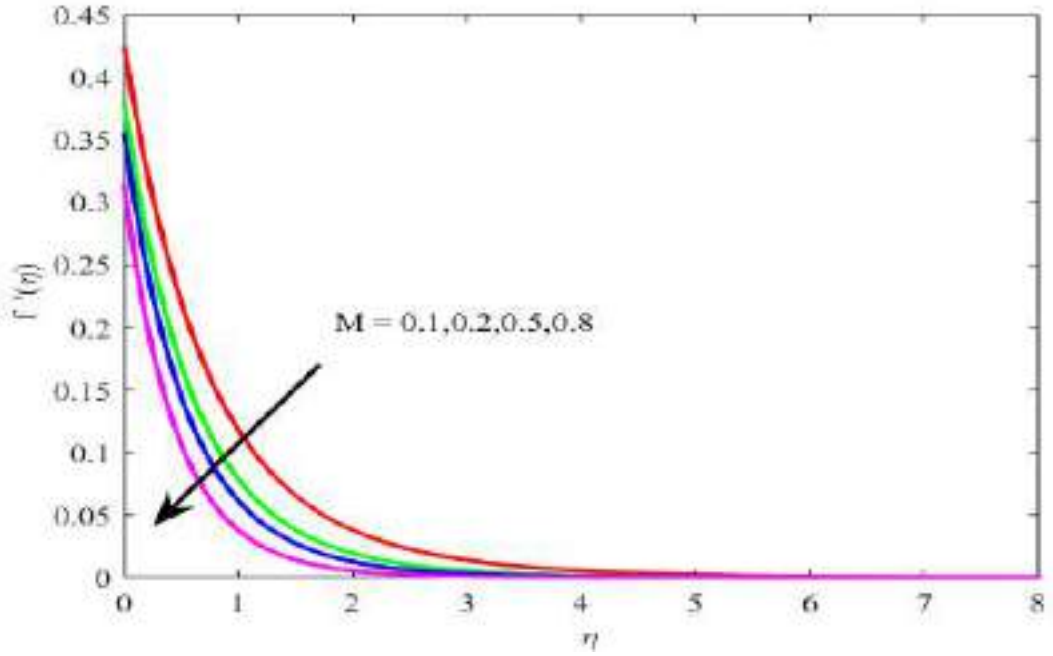

Fig.2 Influence of M on velocity profile.

Fig.2 exhibits the decreasing nature of the velocity profile $f'(\eta)$ and also the boundary layer thickness for higher values of M . This indicates that the increase in M helps to thin of the boundary layer. The velocity profiles exponentially reduce to zero at shorter distances from the sheet for growing values of M .

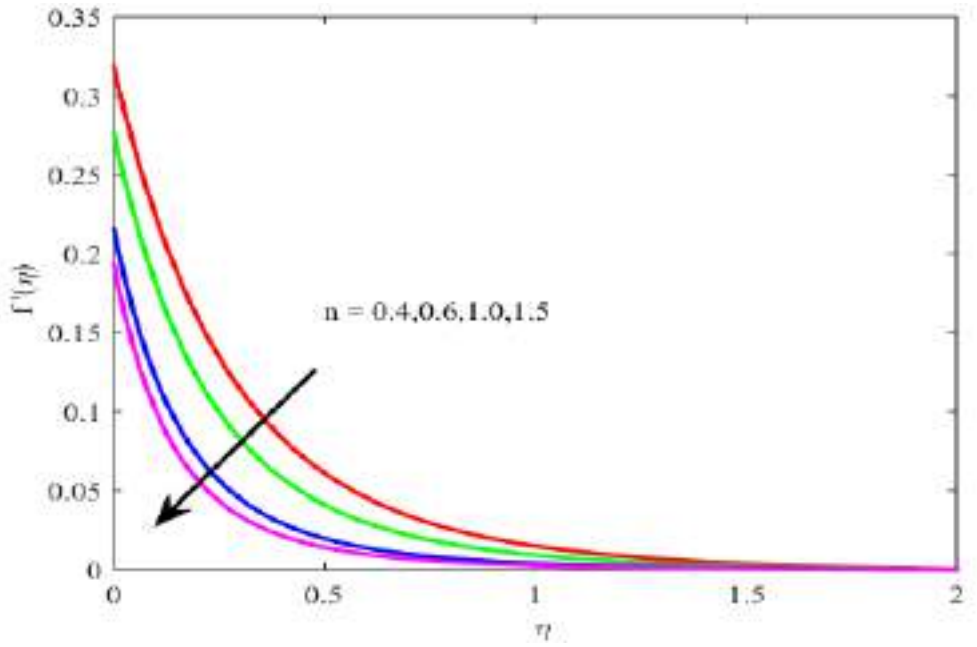

Fig.3 Influence of n on velocity profile.

Fig.3 shows the impact of the curvature parameter on non-dimensional velocity distribution $f'(\eta)$. A rise in the curvature parameter results , decrease in the nondimensional velocity. Resistance force is created by the magnetic field on the fluid in the boundary layer. This force causes restriction to the motion of the fluid. So the magnetic parameter reduces the dimensionless velocity.

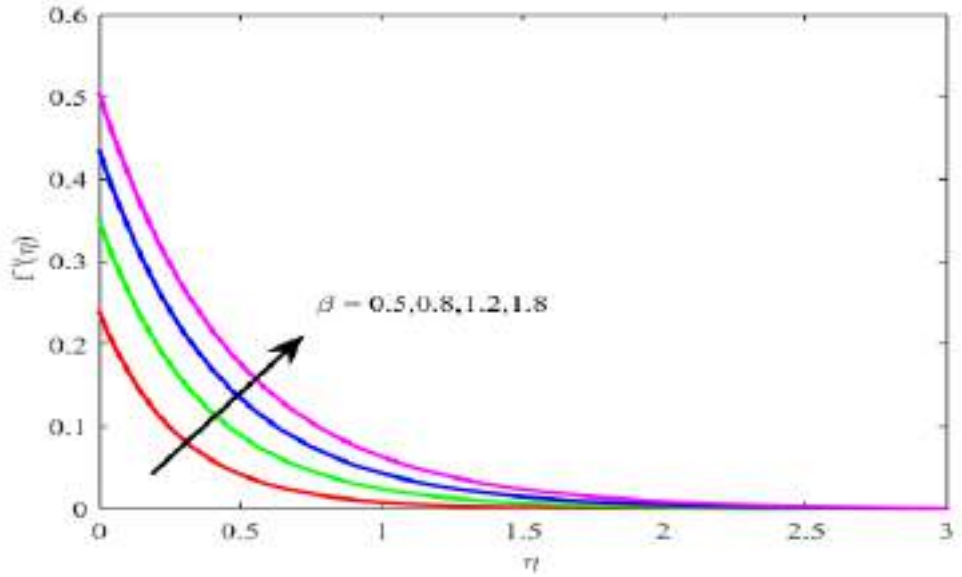

Fig.4 Influence of β on velocity profile.

Fig.4 explicates the increasing nature of velocity profile for rising values of Casson fluid parameter.

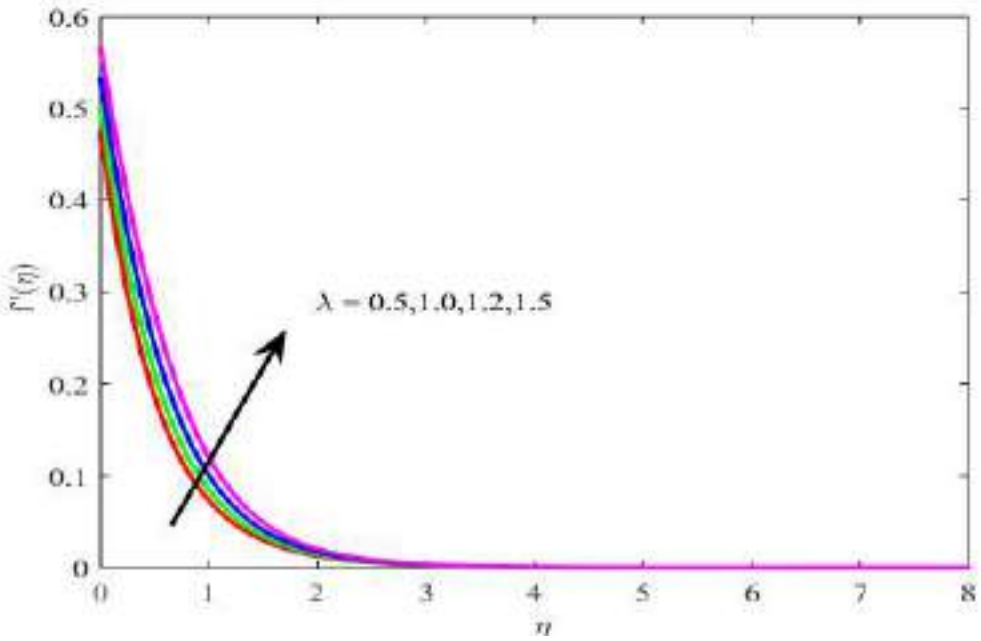

Fig.5 Influence of λ on velocity profile.

Fig.5 illuminates the effect the Wiesenberger number λ on velocity profile. It depicts the velocity profile increased with the increment of λ .

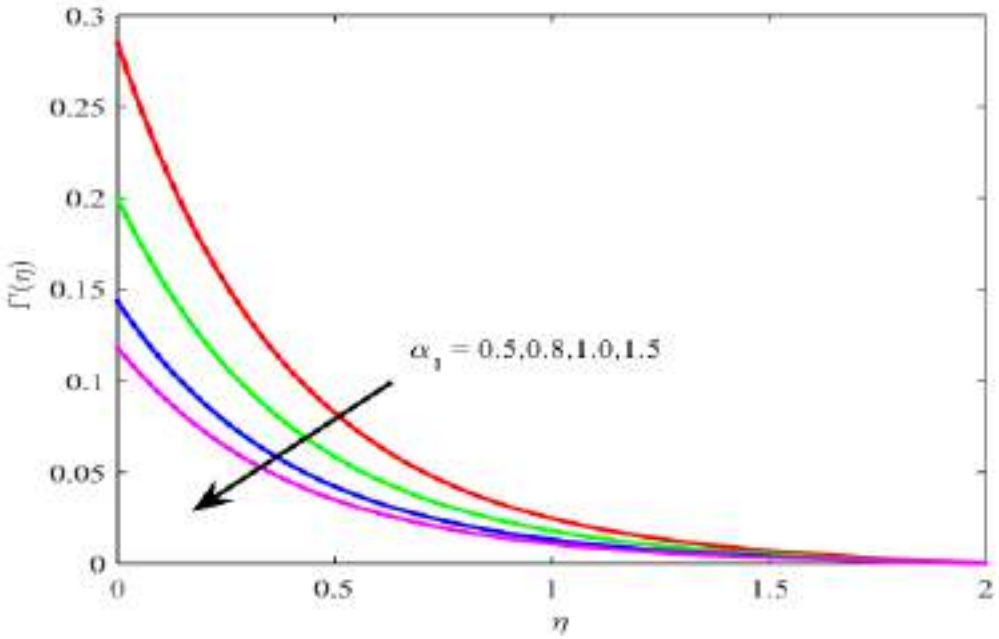

Fig.6 Influence of α_1 on velocity profile.

Fig.6 explains the influence of first-order velocity slip parameter on the dimensionless velocity profile $f'(\eta)$. The dimensionless velocity profile $f'(\eta)$ decreases with increasing values of the first-order velocity slip parameter α_1.

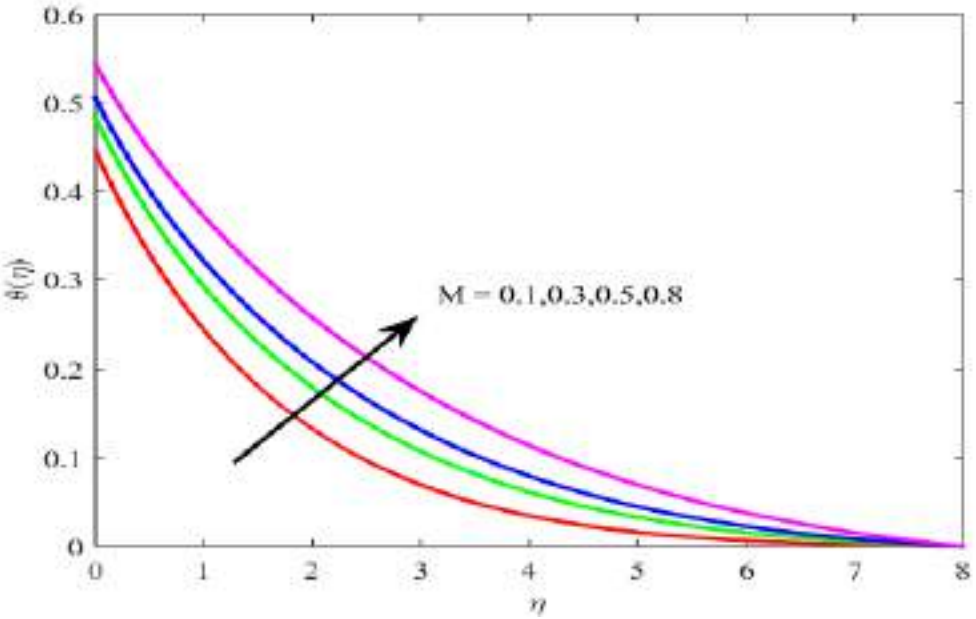

Fig.7 Influence of M on temperature profile.

Fig.7 represents the impact of the magnetic parameter on energy distribution. The effect of magnetic field reduces the fluid velocity whereas it intensifies thermal boundary layer thickness. Thermal energy is defined as an additional work done required for dragging the fluid under the influence of the magnetic field. Thermal energy heats up the conducting fluid and upgrades the temperature profile. Thus, the magnetic field in the flow regime intensifies the thermal boundary layer thickness.

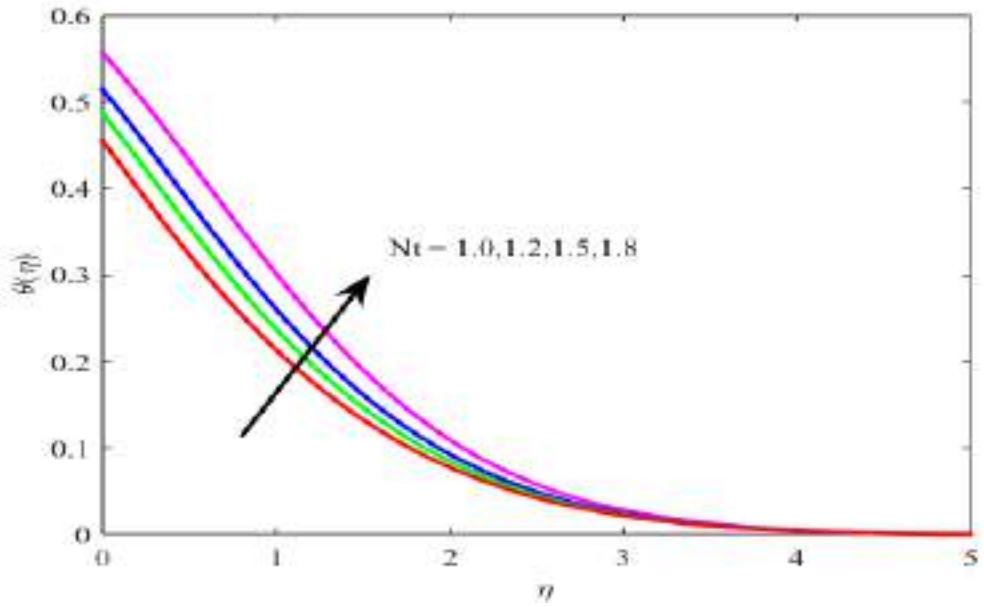

Fig.8 Influence of Nt on temperature profile.

Fig.8 exhibits the influence of the thermophoresis parameter on temperature profile. The energy distribution grows with increment in the values of the thermophoresis parameter.

Conclusion

In the present paper, we have studied the impacts of the thermal radiation, heat source and melting parameter on steady MHD boundary layer of nanofluid under influence of chemical reaction embedded in porous medium. Using the similarity variables, the governing non-linear partial differential equations are transformed into a system of coupled non-linear ODE's and solved numerically by using Runge-Kutta – Fehlberg method with shooting technique. Velocity and temperature increase with increase in heat generation parameter or viscous dissipation. velocity profile, temperature profile and concentration profile decreases for increasing the values of permeability parameter or magnetic field parameter. both local Nusselt number and local Sherwood number increase with Lewis number. The heat source parameter and Eckert number

increases the heat transfer rate, but decreases the mass transfer rate. The skin-friction factor, Nusselt number and Sherwood number decreases with increase in the melting parameter, whereas the effect is opposite for Prandtl number.

References

1 S.U.S. Choi, Enhancing thermal conductivity of fluids with nanoparticle, in: D.A. Siginer

2 C Kleinstreuer and Y Feng, Experimental and theoretical studies of nanofluid thermal conductivity enhancement: a review, Nanoscale Research Letters 2011, 6:229.

3 Yu WH, France DM, Routbort JL, Choi SUS: Review and comparison of nanofluid thermal conductivity and heat transfer enhancements. *Heat Transfer Engineering* 2009, 29: 432–460.

4 Eapen J, Rusconi R, Piazza R, Yip S: The classical nature of thermal conduction in nanofluids. *Journal of Heat Transfer*2010., 132:

5 S.R Chitra and S Sendhilnathan, Investigation on thermal studies of nanofluids related to their applications, Heat Transfer- Asian Research, Vol. 44, No. 5, pp. 420 – 449, 2015.

6 J. Buongiorno Convective transport in nanofluids ASME J. Heat Transfer, 128 (2006), pp. 240–250.

7 H.P. Wang (Eds.), Developments and Applications of Non-Newtonian Flows, *ASME*, New York, Vol. FED 231, pp. 99-105, 1995.

8 F Mabood., W.A Khan and A.I.M Ismail, MHD boundary layer flow and heat transfer of nanofluids over a nonlinear stretching sheet: A numerical study, Journal of Magnetism and Magnetic Materials, Vol.374, No. 15, pp. 569 – 576. 2015.

9 M.A.A. Hamad Analytical solution of natural convection flow of a nanofluid over a linearly stretching sheet in the presence of magnetic field Int. Commun. Heat Mass Transfer, 38 (2011), pp. 487–492.

10 W. Ibrahim, B. Sankar, M.M. Nandeppanavar, MHD stagnation point flow and heat transfer due to nanofluid towards a stretching sheet, Int. J. Heat Mass Transfer, 56 (2013), pp. 1–9.

11 D Srinivasacharya., M Upendar and K Venumadhav, MHD boundary layer flow of a nanofluid past a wedge, International Conference on Computational Heat and Mass Transfer, Procedia Engineering 127 (2015) 1064 – 1070

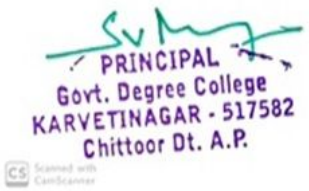

INTERNATIONAL JOURNAL OF MULTIDISCIPLINARY EDUCATIONAL RESEARCH
ISSN:2277-7881; IMPACT FACTOR :6.514(2020); IC VALUE:5.16; ISI VALUE:2.286
Peer Reviewed and Refereed Journal: VOLUME:9, ISSUE:11(6), November:2020

TOURISM IN INDIA- IMPACT & INITIATIVES

[1]P. Revathi Reddy and [2]Dr.S.Vijayulu Reddy
[1]Lecturer in History, Government Degree College, Naidupet.
Affiliated to VS University, Nellore &
[2]Reader in Commerce & Vice Principal, Government Degree College, Naidupet.

Abstract

Travel & Tourism creates jobs, drives exports, and generates prosperity across the world. Today tourism is the largest service industry in India, with a contribution of 6.23 per cent to the national Gross Domestic Product and providing 8.78 per cent of the total employment. Foreign Tourist Arrivals (FTA) crossed the 10 million milestone in 2017 and the growth trend is expected to continue over the coming years. The introduction of E-Visa has led to a strong surge in FTAs which extended to citizens from 166 countries for visit to India through 28 international airports. Key initiatives undertaken by Government of India, Ministry of Tourism, which includes launching of 'Incredible India 2.0 campaign' with market specific content and advertising for tourism development in India. The major challenges faced by the Indian tourism industry are deficiencies in infrastructure like sanitation, living facilities, hotels, etc., and inadequate connectivity between cities and tourist locations and security issues etc. According to the World Travel and Tourism Council, India will be a tourism hotspot from 2009-2018, having the highest 10-year growth potential. Moreover, India has been ranked the "best country brand for value-for-money" in the Country Brand Index survey.

Keywords: GDP, FTA, Incredible India 2.0 Campaign, E-Visa.

1. Introduction

Tourism is one of the powerful operators of employment and wealth globally. The activity of tourism in various countries is reflected the most significant than creation concerning to the financial characteristics as well as social impacts. For a growth of economy tourism is an exceptional facilitator that's why it is a vital part in macroeconomic level. This business is imperative to force labour and is essential cause of government's revenues. As one of the world's largest economic sectors, Travel & Tourism creates jobs, drives exports, and generates prosperity across the world. The sector, comprised of a wide range of industries, aims to serve and support domestic, international, business and leisure visitors. Companies, large and small, in industries ranging from accommodation and transportation to food & beverage, retail and culture and sports & recreation, all strive to create products and services that bring people together, support communities and celebrate the wonders that our world can offer.

In its annual analysis quantifying the global economic and employment impact of Travel & Tourism in 185 countries and 25 regions, the World Travel & Tourism

Council's (WTTC) research reveals that the sector accounted for 10.4 per cent of global GDP and 319 million jobs, or 10 per cent of total employment in 2018. The division of overall spend is firmly weighted towards the leisure market, which represented 78.5 per cent of the total compared with 21.5 per cent for business spend, and the sector accounted for 6.5 per cent of total global exports and 27.2 per cent of total global service exports. Domestic tourism, which represented 71.2 per cent of all tourism spending in 2018 and had the strongest growth in developing nations, continues to support opportunities by spreading development and regional economic benefits and building national pride.

2. Importance of tourism industry

- **Sources of foreign exchange earnings:**Industry of tourism is the key effective type of business worldwide.
- **Employment Opportunities:**This industry is also one of the significant segments. It creates opportunities related to employment. It offers services to inexperienced, pre-nominal and experienced manpower. Director, labour etc are the individual or efforts necessary in the industry of tourism.
- **Sources of public as well as private income:**Industry of tourism is the main cause of earnings for public along with private sector government sales tax, service tax and charges tax etc. which is recognized as government proceeds is the revenue of community. Handicraft, arts etc are the stuffs that fascinate tourist and majority of them purchase them and the seller make some profit which is called private earnings.
- **Cultural Exchange:**Business of tourism accommodates social interchange tourist bring over several ethnic perceptions of other states wherever they visit. Native individuals can pick up their linguistic, skill, talent, values etc and vice versa.

3. Present scenario of Tourism in India

Today tourism is the largest service industry in India, with a contribution of 6.23 per cent to the national Gross Domestic Product (GDP) and providing 8.78 per cent of the total employment. India witnesses' more than 5 million annual Foreign Tourist Arrivals and 562 million domestic tourism visits. The tourism industry in India generated about US$100 billion in 2008 and that is expected to increase to US$275.5 billion by 2018 at a 9.4 per cent annual growth rate. The Ministry of Tourism is the nodal agency for the development and promotion of tourism in India and maintains the *"Incredible India"* campaign.

According to World Travel and Tourism Council, India will be a tourism hotspot from 2009-2018, having the highest 10-year growth potential. As per the Travel and Tourism Competitiveness Report 2017 by the World Economic Forum, India is ranked 11th in the Asia Pacific region and 62nd overall, moving up three places on the list of the world's attractive destinations. It is ranked the 14th best tourist destination for its natural resources and 24th for its cultural resources, with many *World Heritage Sites*,

both natural and cultural, rich fauna, and strong creative industries in the country. India also bagged 37th rank for its air transport network. The India travel and tourism industry ranked 5th in the long-term (10-year) growth and is expected to be the second largest employer in the world by 2019.

Moreover, India has been ranked the "best country brand for value-for-money" in the Country Brand Index (CBI) survey conducted by *Future Brand*, a leading global brand consultancy. India also claimed the second place in CBI's "best country brand for history", as well as appears among the top 5 in the best country brand for authenticity and art & culture, and the fourth best new country for business. India made it to the list of "rising stars" or the countries that are likely to become major tourist destinations in the next five years, led by the United Arab Emirates, China, and Vietnam.

Foreign Tourist Arrivals crossed the 10 million milestone in 2017 and the growth trend is expected to continue over the coming years. However, consumption by domestic tourists remains the key strength of the sector in India, much stronger than the global average. The segment is expected to grow further with growing disposable income, increasing inclination towards travelling across age groups and emergence of new destinations as well as new themes of tourism. India also follows the global trend in terms of higher spending on leisure tourism as compared to business spending. The top 10 source countries accounted for 65.80 per cent of the total inbound tourist flows in 2017, which includes Bangladesh, United States, United Kingdom, Canada and Australia. Foreign tourist arrivals from most of the top source countries grew during the last few years. China, the largest market for outbound tourism, however witnessed a marginal dip. The introduction of E-Visa has led to a strong surge in Foreign Tourist Arrivals since its launch in September, 2014. This scheme has been extended to citizens from 166 countries for visit to India through 28 international airports and 5 sea ports. In 2018, 2.37 million foreign tourists availed the E-Visa facility which represents 39.4 per cent increase over 2017.

Diverse portfolio of tourism offerings including traditional and emerging themes of tourism, including Nature-based, Heritage & Cultural, Religious, Adventure, Medical & Wellness, MICE and Wedding, among others have been a key attraction for domestic and foreign tourists. Strong domestic demand and economic growth, price competitive offerings, infrastructure development, and emergence of new destinations and niche tourism products will continue to drive the growth of the industry in the near future. The Government has been actively working towards tapping plethora of opportunities available in the sector to actualize its true potential. Several initiatives such as rapid implementation of Swadesh Darshan and PRASHAD schemes, E-Visa and Adventure Tourism Guidelines, among others coupled with promotional activities such as Incredible India 2.0 campaign and India Tourism Mart 2018 have immensely benefited the sector. Going forward, there is a greater need for the Government and the private sector to collaborate for successful conceptualization and implementation of developmental initiatives for the sector. The industry has to collectively work with the Government towards thematic development of the destinations and skilling of local

communities. There is also a need for intervention in conservation and promotion of our natural resources, heritage and traditional arts & culture. Technology can be a key enabler and play a critical role in unprecedented growth of the sector.

Tourism in India has traditionally been driven by domestic visitors. Major share of tourist footfall and tourism spending can be attributed to domestic travellers. The overall number of tourist is on the rise in India. In 2017, total number of domestic tourist visits (DTVs) to states and Union Territories stood at 1652.5 million, registering a growth of 2.3 per cent over 2016. Foreign Tourist Arrivals (FTAs) crossed the 10 million milestone in 2017 with a total of 10.04 million tourists visiting India, registering a growth of 14 per cent over 2016. During Jan-Nov 2018, the FTA was 9.37 million, registering a growth of 5.6 per cent over the same period in 2017. However, India still has a considerably small share of FTAs in world's International Tourists arrivals, accounting for nearly 0.76 per cent in 2017. The Government of India has set a target of increasing this share to 1 per cent by 2020 and 2 per cent by 2025. The introduction of E-Visa has led to a strong surge in FTAs. In 2017, 1.7 million foreign tourists availed this option representing 16.9 per cent of total FTAs. New Delhi and Mumbai airport together accounted for 63.7 per cent of these tourists.

4. Tourist Attractions in India

India is a country known for its lavish treatment to all visitors, no matter where they come from. Its visitor-friendly traditions, varied life styles and cultural heritage and colourful fairs and festivals held abiding attractions for the tourists. The other attractions include beautiful beaches, forests and wild life and landscapes for eco-tourism; snow, river and mountain peaks for adventure tourism; technological parks and science museums for science tourism; centres of pilgrimage for spiritual tourism; heritage, trains and hotels for heritage tourism. Yoga, ayurveda and natural health resorts and hill stations also attract tourists. The Indian handicrafts particularly, jewellery, carpets, leather goods, ivory and brass work are the main shopping items of foreign tourists. It is estimated through survey that nearly forty per cent of the tourist expenditure on shopping is spent on such items. Despite the economic slowdown, *medical tourism* in India is the fastest growing segment of tourism industry, according to the market research report "Booming Medical Tourism in India". The report adds that India offers a great potential in the medical tourism industry. Factors such as low cost, scale and range of treatments provided in the country add to its attractiveness as a medical tourism destination.

5. Key Government Initiatives to Promote Inbound Tourism

Some of the recent initiatives taken by the Government to boost tourism include grant of export house status to the tourism sector and incentives for promoting private investment in the form of Income Tax exemptions, interest subsidy and reduced import duty. The hotel and tourism-related industry has been declared a high priority industry for foreign investment which entails automatic approval of direct investment up

to 51 per cent of foreign equity and allowing 100 per cent non-resident Indian investment and simplifying rules regarding the grant of approval to travel agents, tour operators and tourist transport operators.

The first-ever Indian Tourism Day was celebrated on January 25, 1998. The Year 1999 was celebrated as *Explore India Millennium Year* by presenting a spectacular tableau on the cultural heritage of India at the Republic Day Parade and organising India Tourism Expo in New Delhi and Khajuraho. Moreover, the campaign '*Visit India Year 2009'* was launched at the International Tourism Exchange in Berlin, aimed to project India as an attractive destination for holidaymakers. The government joined hands with leading airlines, hoteliers, holiday resorts and tour operators, and offered them a wide range of incentives and bonuses during the period between April and December, 2009.

The Government's developmental agenda is to provide inclusive growth and ensure a future with quality jobs. Travel & Tourism, which already supports one in every ten jobs on the planet, is a dynamic engine of employment opportunity. Moreover, one in every five jobs created during the last 5 years has been linked to Travel & Tourism. Government efforts are now focused upon fast track infrastructure development and promoting tourism digitally. Key initiatives undertaken by Government of India which will foster growth of Tourism industry in India are as under:

Ministry of Tourism

- E-Visa facility extended to 166 countries with relaxed application window, duration and number of entry norms.
- Launched Incredible India 2.0 campaign with market specific content and advertising.
- Planned to set up 5 Special Tourism Zones in partnership with states.
- New National Tourism Policy to be launched.
- Under Swadesh Darshan scheme, the Government has identified 15 circuits on specific themes for development. During 2018-19, a total of 7 projects worth INR 384.67 Cr were sanctioned under the scheme.
- In September 2018, first ever India Tourism Mart 2018 was organized in partnership with Federation of Associations in Indian Tourism and Hospitality (FAITH)
- Launched 'Swachh Paryatan Mobile App' & 24x7 Tourist Helpline in 12 international languages.

Ministry of Civil Aviation

- Civil Aviation Policy 2016 for enhancing connectivity by making air travel safe, secure and affordable
- Six airports across major cities being developed under Public-Private Participation(PPP)
- UDAN scheme (UdeDesh Ka AamNagarik) – low cost flights for boosting regional connectivity, launch of dedicated Airline Service to Northeast states

- ❖ Encouragement to Seaplanes and Helicopter services for tourism operations.

Ministry of Railways

- ❖ IRCTC: Dedicated agency to promote rail tourism
- ❖ Tourist trains: promoting pilgrimage and heritage circuits through railways
- ❖ Semi high speed trains like Gatimaan Express and Tejas Express for enhanced connectivity between key tourism destinations
- ❖ Redevelopment of stations for increased tourist amenities

Ministry of Shipping

- ➢ Development of 78 lighthouses for tourism under PPP
- ➢ Action plan for development of cruise tourism & Cruise Tourism Policy

The growth in India's travel & tourism sector has largely been driven by domestic tourists. Foreign tourists still account for a limited share as compared to some of the top ranking countries. The Government of India intends to achieve the ambitious target of 1 per cent foreign tourist arrivals in world's international tourist arrivals by 2020 and increase it to 2 per cent by 2025. In 2017, India's share stood at 0.76 per cent, which highlights that there is a potential gap that needs to be bridged. In order to achieve this target and make India a Tourism Superpower, coordinated and concerted efforts on multiple fronts will be required.

6. Initiatives to be implemented to promote tourism

- ➢ ***Creation of National Tourism Authority & Advisory Council***: A central level body can be created under the ambit of Ministry of Tourism which includes representatives from the Government and private sector. The private sector representatives should include experts from different tourism segment, including traditional and emerging, so as to incorporate specific inputs for thematic development. The body should also include representatives from other ministries such as Ministry of Shipping; Ministry of Environment, Forest & Climate Change, etc. for greater coordination. The advisory council will provide inputs for policy level decision making and also be approving authority for large scale projects.
- ➢ ***Incentivize Private Sector Participation***: Government should incentivize private players to invest in un-served/ under-served tourism projects. Further, a different incentive structure can be adopted for sustainable development of the lesser explored destinations. For instance, interest subvention scheme can be introduced for small tourism projects like community homestays, RO-RO and boat operators.
- ➢ ***Greater Coordination at State Level:*** There is a need for focused initiatives towards prioritizing Tourism sector across all levels of Government. While the Centre needs to finalize the National Tourism Policy, States will remain the driving force behind implementation of tourism developmental initiatives in their respective regions. It is therefore important for states to have greater coordination between policy-roadmap-budget for effective implementation and timely completion of initiatives.

- ***Leveraging Social Media to Boost Inbound Tourism:*** Social media should be leveraged to promote highly customized content based on user behaviour. Social media influencers, particularly travel bloggers on Instagram, have huge following. An annual conclave of such influencers can be organized in India along with personalized tours for them to promote India's tourist destinations through their channels. Content proliferation through such influencers will reach to a large and targeted segment of potential travellers.
- ***Technology Penetration in Tourism Sector:*** Technologies such as Big Data Analytics and Artificial Intelligence should be employed to deliver insights into consumer behaviour, spending pattern, duration of stay, preferred destinations according to region/ country of origin/ age group, etc. These insights should be used to curate targeted promotion & publicity campaigns. Further, creation of a cashless ecosystem for tourists and technologies like Augmented Reality (AR) and Virtual Reality (VR), Internet of Things (IoT), wearable devices for tourists etc. can be utilized to enhance service quality and delivery leading to enhanced tourist experience, effective promotion and increased sense of security among tourists.
- ***Combined VISA Option:*** India is largely a long-duration destination for foreign travellers. Tourist destinations with good air connectivity may be promoted as short-haul destinations. Further, India can work with other member countries of BIMSTEC, SAARC and ASEAN to offer 'Combined Visa'. Such visa will result in conversion of stopovers to short-haul visits and will also add India on itinerary of tourists on long visits to the South Asian region.
- ***Focus on North East India***: With the implementation of RCS (Regional Connectivity Scheme) UDAN scheme, air connectivity in North East has received much needed boost. Except for Guwahati, the hospitality industry in rest of North East is largely dominated by local players with smaller inventories and limited variety of product offerings. Thus, there is an urgent need to focus towards development of quality accommodation infrastructure across the region to unlock the true potential of North East.

7. Major Challenges in Tourism Sector in India

- ***A cumbersome process for Visa facility:*** Many visitors in India find the e-visa facility, the process of applying for a visa as a cumbersome one.
- ***Limited entry on e-Visa:*** Limited number of repeat visits allowed under medical e-visa and number of accompanying persons. All the three conditions given above, affects the entry process of tourists to the country, hampering the tourism sector in India.
- ***Infrastructure and connectivity:*** Deficiencies in infrastructure like sanitation, living facilities, hotels, etc., and inadequate connectivity hamper tourist visits to heritage sites.
- ***Advertisement and marketing:*** A low degree of marketing strategy is a major concern for tourist places. Also, the campaigns for the places are poorly managed. All these things affect the tourism industry of the region.

- ***Safety:*** Tourists have frequently been mugged and robbed or cheated in India and also have returned without any justice.
- ***Sanitation and health:*** Lack of sanitation in cities has caused a negative impact on Indian food and public health care.
- ***Access:*** Certain areas of India still lack electricity, access, and proper rest houses. Even access to information to domestic and foreign tourists is not at ease.

8. Conclusion

Tourism not only creates jobs in the tertiary sector, it also encourages growth in the primary and secondary sectors of industry. Hence, it is high time, the government should encourage the participation of the private sector in a big way for the all round development of the tourism sector that has the potential to act as the key driver of inclusive growth. With increasing tourist inflows over the past few years, it is a significant contributor to Indian economy as well. Rising income levels and changing lifestyles, development of diverse tourism offerings and policy and regulatory support by the government are playing a pivotal role in shaping the travel and tourism sector in India.

9. References

- www.incredibleindia.org
- Tourism in India -Wikipedia
- www.ibef.org
- A Review of Tourism Development in India - M.M.Malik , *researchgate.net*, 2014.
- Annual Report 2018-19, Ministry of Tourism, Government of India.

Journal of Thermal Analysis and Calorimetry
https://doi.org/10.1007/s10973-018-7427-0

Volumetric, acoustic and spectroscopic approaches to understand the molecular interactions between 1-butyl-3-methylimidazolium hexafluorophosphate and *N*-vinyl-2-pyrrolidinone

P. Suneetha[1] · T. S. Krishna[2] · M. Gowrisankar[3] · M. Srinivasa Reddy[4] · D. Ramachandran[1]

Received: 22 August 2017 / Accepted: 27 May 2018
© Akadémiai Kiadó, Budapest, Hungary 2018

Abstract

In the present paper, we reported the accurately measured densities (ρ), speed of sound (u) and refractive index (n_D) for the binary mixture of 1-butyl-3-methylimidazolium hexafluorophosphate [Bmim] [PF_6] with *N*-vinyl-2-pyrrolidinone (NVP) as a function of concentration at six temperatures from 298.15 to 323.15 K at atmospheric pressure. From the measured density, speed of sound and refractive index, the excess molar volumes, V_m^E, excess isentropic compressibilities, κ_s^E, excess speeds of sound, u^E, excess molar isentropic compressibility, $K_{s,m}^E$, deviation in refractive index, $\Delta_\phi n_D$ and deviation in molar refraction, ΔR_M have been calculated and satisfactorily fitted using the Redlich–Kister polynomial equation. Partial molar volumes and molar isentropic compressibilities were calculated. Infinite dilution values of these derived thermodynamic properties have also been calculated. Evaluation of refractive index has been carried out by nine mixing rules, to investigate their validity for these mixtures over the entire mole fraction of [Bmim][PF_6] at all investigated temperatures. Comparison of these approaches has been presented in terms of APD. Furthermore, the FTIR measurements of these mixtures are carried out at 298.15 K to study the complex formation between [Bmim][PF_6] and NVP. Changes in the measured and calculated values of the physicochemical parameters as a function of temperature and composition of the mixture were analysed in terms of interactions. The results were used to quantitatively analyse the effects of organic solvent NVP with [Bmim] [PF_6] and compared with other anions of [Bmim].

Keywords 1-Butyl-3-methylimidazolium hexafluorophosphate [Bmim] [PF_6] · *N*-Vinyl-2-pyrrolidinone (NVP) · Excess properties · FTIR spectroscopy

Introduction

New methods of laboratory work as well as new technologies increasingly require the use of solvents with desired properties. The solution may be the use of multicomponent liquid mixtures instead of pure solvents. Physicochemical properties of such systems significantly differ from the properties of their pure components, and

Electronic supplementary material The online version of this article (https://doi.org/10.1007/s10973-018-7427-0) contains supplementary material, which is available to authorized users.

✉ T. S. Krishna
sritadikonda@gmail.com

✉ D. Ramachandran
dittakavirc@gmail.com

[1] Department of Chemistry, Acharya Nagarjuna University, Nagarjuna Nagar, Guntur, Andhra Pradesh 522510, India

[2] Department of Physics, A.S.N. Women's Engineering College, Tenali, Andhra Pradesh 522201, India

[3] Department of Chemistry, J.K.C.C. Acharya Nagarjuna University, Guntur, Andhra Pradesh 522006, India

[4] Department of Chemistry, T.R.R. Government Degree College, Kandukur, Andhra Pradesh 523105, India

their thorough studies provide information not only about the interactions occurring in such systems, but also allow wider application of the investigated mixtures in practice [1]. The authors also show how one can get a lot of thermodynamic data only from the density measurements without the use of complicated and labour-intensive calorimetric methods.

The information of thermo- and physicochemical behaviour of ILs is especially important to plan new inventories including ILs and industrial processes [2]. The ILs are occupying the place of volatile organic compounds because of their negligible vapour pressures. The ILs as recyclable solvents have prompt diminishment in VOC emanations and furthermore to a practical utilization of beginning materials in industry [3].

ILs are specially known as architect solvents in the light of the fact that their properties can be changed to specific applications with interesting mixtures of cations and anions [4]. Apart from changing the cations and anions, an addition of co-solvent to improve the physicochemical properties of these designer solvents is also gaining scientific attention to scientific researchers to discover their novel applications [5–7].

From past 10–15 years, scientists as well as chemists initiated action to address environmental issues in a safe and gainful manner under the name "green chemistry" to highlight the judicious use of chemistry for prevention of pollution through environmentally conscious designing of chemical processes. So, solvents play a wider role in analytical chemistry, product purification, extraction and separation technologies. Therefore, to make chemistry more sustainable in these fields, knowledge of alternative, greener solvents or their mixtures were important in order to replace traditional organic solvents.

There are some critical evaluation criteria for selecting novel working pairs such as to ensure high efficiency of absorption hydrodesulfurization (HDS) to be noncorrosive, to be nontoxic and to ensure secure operation and so on. The determination of the fitting ionic fluid and its capacity to extricate aromatic sulphur compounds is troublesome in these sorts of process. *N*-vinyl-2-pyrrolidinone is one of the particular advantages in decolorizing crude oil free from asphaltic constituents and as an adsorbent for sour gases from crude natural gas [8]. So, the combination mixture makes more advantage in petro-product extraction.

This work is a continuation of our comprehensive study [9, 10] related to the study of acoustic, volumetric and refractive index properties of binary mixtures of ionic liquids with volatile organic compound of *N*-vinyl-2-pyrrolidinone (NVP) with the enhancement of temperature at ambient pressure (0.1 MPa). In spite of importance of properties of ILs with NVP, there is limited information available on the thermodynamic properties of IL mixtures with other fluids, and these properties are still lacking. The present study is therefore undertaken to evaluate the influence of particular specific interactions on the excess properties with the enhancement of temperature, and the presence of anion in the IL and the NVP.

In the present study, we report the densities, ρ, speeds of sound, u and refractive indices, n_D of binary mixtures of [Bmim][PF_6] and NVP, over the entire composition range at temperatures (298.15–323.15) K and at atmospheric pressure. Pure liquids data were taken from our previous papers [9, 11]. Using the experimental data, the excess and excess partial molar volumes of the components at infinite dilution have also been calculated. The variations of these parameters with composition and temperature have been discussed in terms of intermolecular interactions prevailing in these mixtures.

Experimental

Materials

The names, provenances and purities of the solutes used in this work are given in Table 1. The 1-butyl-3-methylimidazolium hexafluorophosphate [Bmim][PF_6] was procured from Iolitec (Germany); the mass fraction purity of the ionic liquids (as stated by the manufacturer) is > 0.99 with less than 100 ppm water content and less than 100 ppm halide ion concentration. In order to reduce the water content to negligible values, vacuum (0.1 Pa) and moderate temperature (60 °C) were applied to [Bmim][PF_6] for several days, prior to use. After drying under vacuum and 60 °C temperature, the water content was found to be within limits specified by the manufacturer (890 KF Titrando, Metrohm, USA) [12].

[BMIM][PF_6] purity was checked through ^{1}H-NMR on an advance DPX400 Bruker initial and after drying is shown in Figures 1S and 2S (*supplementary material*). NMR spectra are well matched with report conducted by Dupont et al. [13, 14] and utilized without further purification.

^{1}H NMR ($CDCl_3$): $\delta = 0.96$ ppm (t, 3H, $J = 7.21$), $\delta = 1.29$ ppm (m, 2H), $\delta = 1.78$ ppm (m, 2H), $\delta = 3.83$ ppm (s, 3H), $\delta = 4.09$ ppm (t, 2H, $J = 7.40$), $\delta = 7.25$ ppm (d, 1H, $J = 3.51$), $\delta = 7.30$ ppm (d, 1H, $J = 5.35$), $\delta = 8.35$ ppm (s, 1H).

In FTIR, three vibrational modes of water were detectable and did not increase much after exposure during a few hours to air. Water molecules were not hydrogen bonded to each other, as in this IL no band was detectable in the range of 3550–3250 cm^{-1}. All these findings are comparable to the existing literature [15]. The intensities of the IL bands did not decrease by more than 1

Table 1 Specification of chemical samples

Chemical name (CAS number)	Source	Initial mass fraction purity	Purification method	Final mass fraction purity	Analysis method	Water mass fraction (ppm)	Water analysis method
[Bmim][PF_6] (174501-64-5)	Iolitech, Germany	> 0.995	Degassed under vacuum	> 0.995	NA	< 40	Karl Fischer
N-Vinyl-2-pyrrolidinone (88-12-0)	Sigma-Aldrich, India	> 0.97	Fractional distillation	> 0.98	GC[a]	< 150	Karl Fischer

[a]Gas chromatography

or 2%. Therefore, it was not possible to quantify the probable small swelling of [Bmim][PF_6] caused by the diffusion of water into the IL and found a good agreement with the literature [16].

NVP was procured from Sigma-Aldrich, USA, with mass fraction purity of 0.97 and was purified by the fractional distillation method under reduced pressure [17]. Purity was checked by gas chromatograph (GC), and water content of NVP was found less than 150 ppm [10]. The sample preparation was done as described in our previous publication [18]. The solutions were prepared by weighing with CPA-225D (Japan) electronic balance, sensitive to ± 0.01 mg. The uncertainty in the mole fraction was estimated to be within ± $1{\cdot}10^{-4}$. In order to avoid water absorption, the ionic liquid was used inside a glove box under argon. The scattered speed of sound values was graphically compared with George et al. [19], with our results in supplementary material, Figure 3S. In our opinion, the differences may be due to the measurement procedure such as ultrasonic interferometer (Mittal Enterprises, New Delhi, India) operated at a fixed frequency of 2 MHz and some of issues such as purity of the NVP (97%). The density of [Bmim][PF_6] was graphically compared with average absolute deviation $\left(\mathrm{AAD} = (100/n)\sum_{i=1}^{n}\left|\rho_{\mathrm{lit}}/\rho_{\mathrm{exp}\,t} - 1\right|\right)$ in Fig. 1 with the literature [20–27] at T = 298.15–323.15 K which agrees with literature values with a maximum absolute deviation less than 0.25%.

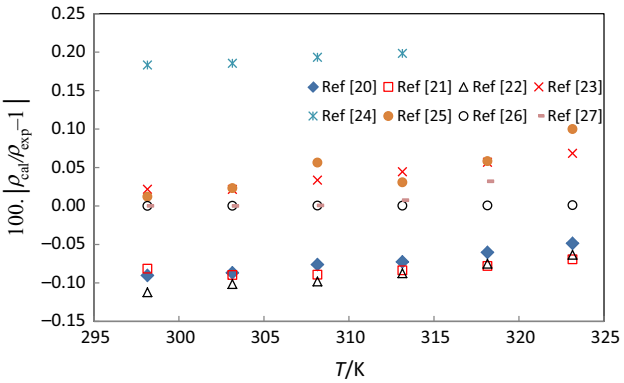

Fig. 1 Graphical comparison density of [Bmim][PF_6] with various researchers [20–27]

Apparatus and procedure

Densities and speed of sound were measured by an Anton Paar DSA 5000 M, high-precision vibrating tube digital densimeter and speed of sound measuring device, with automatic viscosity corrections. The instrument has a built-in thermostat to maintain the temperature between 0 and 70 °C with a precision of ± 0.001 °C. Its piezo frequency is around 3 MHz. The densimeter was calibrated randomly with dry air at atmospheric pressure and triply distilled, freshly degassed and deionized water (ρ = 997.075 kg m^{-3} at 298.15 K) supplied by Anton-Paar as described elsewhere. The standard uncertainties associated with the measurements for temperature, density and speed of sound were estimated to be within ± 0.01 K, ± 0.8 kg m^{-3} and ± 1 m s^{-1}, respectively [28]. A third-order polynomial was used to fit the speed of sound as a function of concentration (b_i), for pure substances and its binary mixture of [Bmim][PF_6] with NVP are listed in Table 1S and Fig 4S (*Supplementary material*).

The refractive indices of pure components and binary mixtures were measured with an automatic digital precision refractometer by Dr. Krenchen Abbemat HP (RXA170 Heavy duty, Anton Paar, Austria) as described elsewhere [29]. The uncertainties in the temperature and refractive index measurements were estimated to be within ± 0.02 K and ± 0.0005, respectively.

FTIR measurements of pure [Bmim][PF_6], NVP and 0.1–0.9 mol fractions of [Bmim][PF_6] + NVP mixtures were carried out with FTIR Spectrometer (Alpha FTIR, Bruker, Germany) with accessory Alpha E by using ATR technique (400–4000) cm^{-1} with 4.0 cm^{-1} resolution to investigate the strength of molecular associations in these mixtures. All spectrums were recorded at room temperature. The IR data were analysed using OPUS 6.5 software.

Theory

Excess properties

To understand the molecular interactions of [Bmim][PF_6] + NVP the thermophysical properties such as density, ρ, speed of sound, u, and refractive index, n_D, were determined over the mole fraction range at temperature range from T/K = 298.15–323.15, at atmospheric pressure and given in Table 2. Excess molar volume (V_m^E), excess isentropic compressibility (κ_s^E), excess molar isentropic compressibility ($K_{s,m}^E$), excess speed of sound (u^E) and deviation refractive index (Δn_D) were calculated from the experimental density, speed of sound and refractive index measurement by the relationships [30–32]:

$$V_m^E = V_m - V_m^{id} \tag{1}$$

$$\kappa_s^E = \kappa_s - \kappa_s^{id} \tag{2}$$

$$K_{S,M}^E = K_{S,M} - K_{S,M}^{id} \tag{3}$$

$$u^E = u - u^{id} \tag{4}$$

The thermodynamic properties of molar volume V_m, the coefficient of thermal expansion, α_p, and the isentropic compressibility, κ_S values are derived directly from the experimental measurements with density ρ, and speed of sound, u.

$$\alpha_p = -\frac{1}{\rho}\left(\frac{\Delta\rho}{\Delta T}\right)_p \tag{5}$$

In this work, α_p values are obtained from a linear dependence of ρ with T. The C_p values of the pure liquids at investigated temperatures have been taken from our previous papers [9, 20].

Excess isobaric thermal expansivity

To extend an understanding of the molecular interaction of the solution during mixing, excess isobaric thermal expansivity was calculated for the investigated composition [33], and to know more the difference between numerical (Eq. 5) and analytical methods (Eq. 6) [34] is of isobaric thermal expansion. For more clarity, authors calculated the excess thermal expansivity (α_p^E).

By analytically, α_p can be calculated as

$$\alpha_p = -\frac{1}{\rho}\left(\frac{\partial\rho}{\partial T}\right)_p \tag{6}$$

$$\alpha_p^E/(K^{-1}) = \alpha_p - \alpha_p^{id} = (\partial V_m/\partial T)_p/V_m - \sum_{i=1}^{2}\phi_i\alpha_{p,i}^* \tag{7}$$

The deviation in refractive index, $\Delta_\phi n_D$, has been calculated on the basis of volume fraction [35] as

$$\Delta_\phi n_D = n_D - \left[\phi_1(n_{D,1})^2 + \phi_2(n_{D,2})^2\right]^{1/2} \tag{8}$$

Molar refraction, R_M, was obtained from experimental refractive index data by using the following expression

$$R_M = \left[\frac{n_D^2 - 1}{n_D^2 + 2}\right]V_m$$

The deviation in molar refraction, ΔR_M, has been calculated by using the following expression [35]

$$\Delta R_M = R - (x_1 R_{M,1} + x_2 R_{M,2}) \tag{9}$$

The values of V_m^E, κ_s^E $K_{s,m}^E$, u^E, ΔR_m as functions of mole fraction, x_1 of [Bmim][PF_6] and temperature for both the systems are presented in Table 3.

The excess values of the above parameters for the mixtures have been fitted to the Redlich–Kister [36] polynomial equation

$$Y^E = x_1 x_2 \sum_{i=1}^{n} A_i(2x_1 - 1)^i \tag{10}$$

where Y^E is V_m^E, κ_s^E, $K_{s,m}^E$ and u^E, $\Delta_\phi n_D$, ΔR_m and α_p^E. The equation coefficients, A_i, obtained by the method of least squares with equal weights assigned to each point were calculated along with the standard deviation σ (Y^E). The coefficients were adjustable parameters for a better fit of the excess functions.

The standard deviation $\sigma(Y^E)$ is calculated using,

$$\sigma(Y^E) = \left(\frac{\sum\left(Y_{exp\,t}^E - Y_{cal}^E\right)^2}{(m-n)}\right)^{1/2} \tag{11}$$

where m is equal to the number of experimental points, n is the number of A_i coefficients considered ($n + 1$ in the present study). The optimal number of A_i coefficients has been determined statistically by performing F-test. If the p value is small, we can accept the null hypothesis. Then only we can consider the F-value. In other words, p value and F-value should both be statistically significant in order to correctly interpret the results. The coefficients, A_i and corresponding standard deviations, σ fit of V_m^E, κ_s^E $K_{s,m}^E$, u^E, $\Delta_\phi n_D$, ΔR_m, α_p^E, standard error, F-values and p values are given in Table 4. The variations of V_m^E, κ_s^E, $K_{s,m}^E$, u^E, $\Delta_\phi n_D$ and ΔR_m and α_p^E with mole fraction, x_1, along with smoothed values from Eq. (10) at studied temperatures are shown graphically in Figs. 2, 4–7, 5S and 6S, respectively.

Table 2 Densities, ρ, speeds of sound, u, refractive index, n_D as a function of mole fraction, x_1 of [Bmim][PF_6] for [Bmim][PF_6] + NVP binary mixtures at the temperatures, T = (298.15–323.15) K and at pressure p = 0.1 MPa

x_1	T/K					
	298.15	303.15	308.15	313.15	318.15	323.15
ρ/(kg m^{-3})						
0.0000 [8]	1039.4	1035.0	1030.6	1026.1	1021.7	1017.3
0.1011	1102.5	1098.2	1094.0	1089.7	1085.4	1081.1
0.2059	1156.1	1151.9	1147.7	1143.5	1139.2	1135.1
0.3019	1197.0	1192.8	1188.7	1184.5	1180.3	1176.2
0.3937	1230.3	1226.2	1222.0	1217.9	1213.7	1209.6
0.5023	1264.0	1259.9	1255.7	1251.6	1247.4	1243.3
0.5840	1286.0	1281.8	1277.6	1273.5	1269.3	1265.2
0.6946	1311.9	1307.8	1303.6	1299.4	1295.2	1291.0
0.7788	1329.3	1325.1	1320.9	1316.7	1312.5	1308.3
0.8707	1346.3	1342.1	1337.9	1333.6	1329.4	1325.2
1.0000 [10]	1367.2	1363.0	1358.7	1354.5	1350.2	1346.0
u/(m s^{-1})						
0.0000 [8]	1521.5	1502.5	1483.7	1465.0	1446.5	1428.1
0.1011	1515.9	1498.9	1481.8	1464.7	1447.8	1431.1
0.2059	1506.0	1490.1	1474.2	1458.3	1442.6	1427.0
0.3019	1496.4	1481.4	1466.3	1451.4	1436.6	1422.0
0.3937	1487.8	1473.5	1459.2	1444.9	1430.9	1416.9
0.5023	1477.6	1463.9	1450.2	1436.7	1423.4	1410.2
0.5840	1470.5	1457.4	1444.3	1431.2	1418.4	1405.7
0.6946	1461.5	1449.1	1436.4	1423.9	1411.6	1399.4
0.7788	1455.7	1443.4	1431.1	1419.0	1407.0	1395.1
0.8707	1449.9	1437.9	1425.8	1414.0	1402.3	1390.8
1.0000 [10]	1443.8	1431.7	1419.8	1408.2	1396.8	1385.6
n_D						
0.0000 [8]	1.5104	1.5081	1.5058	1.5035	1.5012	1.4989
0.1011	1.4953	1.4932	1.4910	1.4889	1.4868	1.4847
0.2059	1.4808	1.4788	1.4769	1.4749	1.4729	1.4710
0.3019	1.4686	1.4667	1.4649	1.4631	1.4612	1.4594
0.3937	1.4578	1.4561	1.4544	1.4526	1.4509	1.4492
0.5023	1.4463	1.4447	1.4430	1.4414	1.4398	1.4382
0.5840	1.4384	1.4369	1.4353	1.4338	1.4323	1.4307
0.6946	1.4290	1.4275	1.4260	1.4246	1.4231	1.4216
0.7788	1.4227	1.4213	1.4198	1.4184	1.4170	1.4155
0.8707	1.4166	1.4153	1.4139	1.4125	1.4111	1.4097
1.0000 [10]	1.4097	1.4084	1.4071	1.4057	1.4043	1.4029

Standard uncertainties s are $s(T)$ = ± 0.01 K, $s(x)$ = ± 1.0 × 10^{-4}, $s(\rho)$ = ± 0.8 kg m^{-3}, $s(u)$ = ± 1 m s^{-1}, $s(n_D)$ = ± 0.0005, $s(T)$ for n_D = ± 0.02 K, and $s(p)$ = ± 1.0 kPa

Partial molar properties

In addition to other volumetric properties (partial molar volumes and partial molar compressibility) $\overline{Y}_{m,1}$ and $\overline{Y}_{m,2}$ of IL and NVP over the entire concentration range in investigated system have been determined using the following equations

$$\overline{Y}_{m,1} = Y_s^E + Y_{m,1}^* + x_2\left(\frac{\partial Y_s^E}{\partial x_1}\right)_{T,p} \quad (12)$$

$$\overline{Y}_{m,2} = Y_s^E + Y_{m,2}^* - x_1\left(\frac{\partial Y_s^E}{\partial x_1}\right)_{T,p} \quad (13)$$

where Y is V or K_s where $Y_{m,1}^*$ and $Y_{m,2}^*$ are the molar components of pure components IL and NVP, respectively.

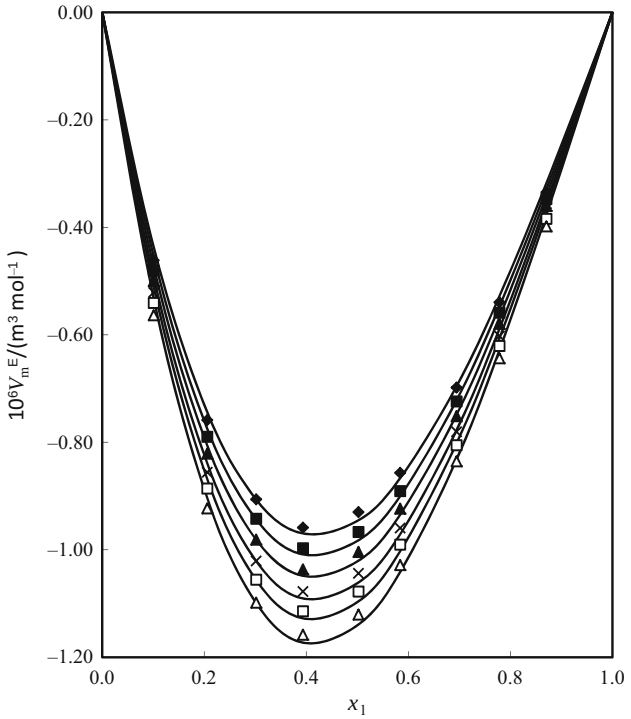

Fig. 2 Plots of excess molar volume, V_m^E versus mole fraction, x_1 of [Bmim][PF_6] for [Bmim][PF_6] + NVP binary mixtures at temperatures, T/K = 298.15, ◆; At T/K = 303.15, ■; T/K = 308.15, ▲; T/K = 313.15, ×; T/K = 318.15, □; T/K = 323.15, Δ. The points represent experimental values, and lines represent values calculated from Eq. (10) using the coefficients given in Table 4

The derivative $(\partial Y_s^E/\partial x_1)_{T,p}$ in Eqs. (12) and (13) was obtained by differentiation, which lead to the following equations for $\overline{Y}_{m,1}$ and $\overline{Y}_{m,2}$.

$$\overline{Y}_{m,1} = \overline{Y}^*_{m,1} + x_2^2 \sum_{i=0}^{j} A_i (1-2x_1)^i - 2x_1 x_2^2 \sum_{i=0}^{j} A_i (1-2x_1)^{i-1} \quad (14)$$

$$\overline{Y}_{m,2} = \overline{Y}^*_{m,2} + x_1^2 \sum_{i=0}^{j} A_i (1-2x_1)^i + 2x_2 x_1^2 \sum_{i=0}^{j} A_i (1-2x_1)^{i-1} \quad (15)$$

$Y^*_{m,1}$ and $Y^*_{m,2}$ are the molar properties of pure components, and the excess partial molar properties are calculated by the following relations [37, 38],

$$\overline{Y}^E_{m,i} = Y^E_m + (1-x_1)\left(\partial Y^E_m/\partial x_i\right) \quad (16)$$

We are interested to evaluate the partial molar properties of [Bmim][PF_6] at infinite dilution ($x_1 = 0$) in NVP, and the partial molar properties of NVP at infinite dilution ($x_2 = 0$) in [Bmim][PF_6]. Therefore, $\overline{Y}^\circ_{m,1}$ is obtained by setting $x_1 = 0$ which leads to

$$\overline{Y}^\circ_{m,1} = Y^*_{m,1} + \sum_{i=0}^{n} A_i (-1)^i \quad (17)$$

Similarly, setting $x_2 = 0$ leads to

$$\overline{Y}^\circ_{m,2} = Y^*_{m,2} + \sum_{i=0}^{n} A_i \quad (18)$$

here $\overline{Y}^\circ_{m,1}$ and $\overline{Y}^\circ_{m,2}$ represent the partial molar properties of [Bmim][PF_6] at infinite dilution in NVP and the partial molar properties of NVP at infinite dilution in [Bmim][PF_6], respectively.

Excess partial molar properties at infinite dilution $\overline{Y}^{\circ,E}_{m,i}$ for each component in binary liquid mixtures are evaluated through relations

$$\overline{Y}^{\circ,E}_{m,1} = \overline{Y}^\circ_{m,1} - Y^*_{m,1} \quad (19)$$

$$\overline{Y}^{\circ,E}_{m,2} = \overline{Y}^\circ_{m,2} - Y^*_{m,2} \quad (20)$$

The variations of $\overline{V}^E_{m,1}$ and $\overline{V}^E_{m,2}$; and $\overline{K}^E_{s,m,1}$ and $\overline{K}^E_{s,m,2}$ with composition and temperature are listed in Tables 3S–4S as given in *supplementary material* and are presented graphically in Figs. 8 and 9, respectively.

The values of partial molar properties, $\overline{Y}^\circ_{m,1}$ and $\overline{Y}^\circ_{m,2}$, of [Bmim][PF_6] and NVP at infinite dilution are calculated by using Eqs. (17)–(18), and the excess partial molar properties, $\overline{Y}^{\circ E}_{m,1}$ and $\overline{Y}^{\circ E}_{m,2}$ at infinite dilution are calculated using Eqs. (19) and (20). The values of $\overline{V}^\circ_{m,1}$, $V^*_{m,1}$, $\overline{V}^{\circ E}_{m,1}$, $\overline{V}^\circ_{m,2}$, $V^*_{m,2}$ and $\overline{V}^{\circ E}_{m,2}$; and $\overline{K}^\circ_{s,m,1}$, $K^*_{s,m,1}$, $\overline{K}^{\circ E}_{s,m,1}$, $\overline{K}^\circ_{s,m,2}$, $K^*_{s,m,2}$ and $\overline{K}^{\circ E}_{s,m,2}$ for the binary mixtures at each investigated temperature are listed in Tables 5 and 6, respectively.

Results and discussion

Excess properties

The experimental values of densities (ρ), speed of sound (u), refractive index (n_D) were used to calculate excess properties such as excess molar volume (V^E_m), isentropic compressibility (κ^E_s), excess molar isentropic compressibility ($K^E_{s,m}$), excess speed of sound (u^E), deviation in refractive index $\Delta_\phi n_D$, and deviations in molar refractive index (ΔR_m) of the binary mixtures over the entire composition range and at 298.15–323.15 K temperatures are listed in Table 2. The variation of pure values of ρ, u and n_D with temperature is found to be linear, whereas variation of ρ, u and n_D with mole fraction is found to be nonlinear.

Table 3 Excess molar volume (V_m^E), excess isentropic compressibility (κ_s^E), excess molar isentropic compressibility ($K_{s,m}^E$), excess speed of sound (u^E), deviation in refractive index ($\Delta_\phi n_D$), deviation in molar refraction (ΔR_M) and excess isobaric expansivity (α_p^E) as a function of mole fraction, x_1 of [Bmim][PF_6] for [Bmim][PF_6] + NVP at the temperatures T = (298.15–323.15) K at pressure p = 0.1 MPa

x_1	V_m^E 10^6/m^3 mol^{-1}	κ_s^E 10^{10}/m^2 N^{-1}	$K_{s,m}^E$ 10^{14}/m^5 N^{-1} mol^{-1}	u^E 10^{-2}/m s^{-1}	$10^6.\Delta R_M$/m^3 mol^{-1}	$10^2.\Delta_\phi n_D$	α_p^E/kK^{-1}
298.15 K							
0.1011	− 0.461	− 0.109	− 0.141	0.174	0.071	− 0.117	− 2.137
0.2059	− 0.759	− 0.159	− 0.224	0.259	0.104	− 0.442	− 3.886
0.3019	− 0.906	− 0.170	− 0.260	0.282	0.102	− 0.639	− 5.045
0.3937	− 0.959	− 0.163	− 0.266	0.272	0.076	− 0.540	− 5.745
0.5023	− 0.930	− 0.139	− 0.246	0.233	0.025	− 0.708	− 6.047
0.5840	− 0.857	− 0.116	− 0.217	0.194	− 0.019	− 0.440	− 5.893
0.6946	− 0.698	− 0.081	− 0.163	0.134	− 0.070	− 0.596	− 5.162
0.7788	− 0.540	− 0.054	− 0.116	0.089	− 0.092	− 0.492	− 4.200
0.8707	− 0.335	− 0.028	− 0.065	0.045	− 0.086	− 0.196	− 2.750
303.15 K							
0.1011	− 0.481	− 0.115	− 0.150	0.178	0.064	− 0.115	− 2.204
0.2059	− 0.790	− 0.169	− 0.240	0.266	0.095	− 0.434	− 4.012
0.3019	− 0.942	− 0.182	− 0.278	0.291	0.092	− 0.629	− 5.216
0.3937	− 0.997	− 0.174	− 0.286	0.282	0.066	− 0.530	− 5.945
0.5023	− 0.967	− 0.150	− 0.265	0.244	0.016	− 0.696	− 6.263
0.5840	− 0.891	− 0.125	− 0.234	0.203	− 0.026	− 0.431	− 6.108
0.6946	− 0.724	− 0.088	− 0.177	0.142	− 0.074	− 0.586	− 5.354
0.7788	− 0.559	− 0.060	− 0.127	0.096	− 0.094	− 0.484	− 4.359
0.8707	− 0.347	− 0.031	− 0.072	0.049	− 0.087	− 0.192	− 2.855
308.15 K							
0.1011	− 0.500	− 0.122	− 0.160	0.182	0.059	− 0.110	− 2.273
0.2059	− 0.821	− 0.179	− 0.256	0.273	0.087	− 0.424	− 4.143
0.3019	− 0.981	− 0.194	− 0.297	0.299	0.083	− 0.616	− 5.392
0.3937	− 1.037	− 0.186	− 0.305	0.290	0.058	− 0.516	− 6.151
0.5023	− 1.004	− 0.160	− 0.284	0.252	0.011	− 0.681	− 6.485
0.5840	− 0.924	− 0.134	− 0.251	0.211	− 0.029	− 0.419	− 6.328
0.6946	− 0.751	− 0.094	− 0.191	0.149	− 0.076	− 0.573	− 5.550
0.7788	− 0.580	− 0.064	− 0.137	0.100	− 0.094	− 0.473	− 4.520
0.8707	− 0.360	− 0.034	− 0.077	0.052	− 0.086	− 0.186	− 2.961
313.15 K							
0.1011	− 0.521	− 0.129	− 0.170	0.184	0.054	− 0.105	− 2.345
0.2059	− 0.856	− 0.190	− 0.271	0.277	0.081	− 0.413	− 4.281
0.3019	− 1.021	− 0.205	− 0.316	0.305	0.077	− 0.600	− 5.577
0.3937	− 1.078	− 0.197	− 0.324	0.297	0.054	− 0.500	− 6.366
0.5023	− 1.044	− 0.170	− 0.302	0.259	0.008	− 0.662	− 6.718
0.5840	− 0.960	− 0.142	− 0.267	0.218	− 0.030	− 0.403	− 6.558
0.6946	− 0.780	− 0.100	− 0.203	0.154	− 0.075	− 0.557	− 5.756
0.7788	− 0.602	− 0.068	− 0.147	0.104	− 0.092	− 0.460	− 4.689
0.8707	− 0.373	− 0.036	− 0.083	0.054	− 0.084	− 0.178	− 3.074
318.15 K							
0.1011	− 0.541	− 0.137	− 0.181	0.188	0.049	− 0.101	− 2.404
0.2059	− 0.886	− 0.201	− 0.289	0.284	0.073	− 0.403	− 4.396
0.3019	− 1.056	− 0.217	− 0.336	0.313	0.070	− 0.587	− 5.733
0.3937	− 1.114	− 0.209	− 0.346	0.306	0.047	− 0.487	− 6.551
0.5023	− 1.078	− 0.180	− 0.322	0.267	0.004	− 0.647	− 6.920
0.5840	− 0.990	− 0.151	− 0.285	0.225	− 0.033	− 0.390	− 6.760

Table 3 (continued)

x_1	V_m^E 10^6/m^3 mol^{-1}	κ_s^E 10^{10}/m^2 N^{-1}	$K_{s,m}^E$ 10^{14}/m^5 N^{-1} mol^{-1}	u^E 10^{-2}/m s^{-1}	$10^6.\Delta R_M$/m^3 mol^{-1}	$10^2.\Delta_\phi n_D$	α_p^E/kK^{-1}
0.6946	− 0.805	− 0.107	− 0.217	0.160	− 0.076	− 0.545	− 5.937
0.7788	− 0.621	− 0.073	− 0.157	0.109	− 0.092	− 0.450	− 4.840
0.8707	− 0.384	− 0.039	− 0.089	0.057	− 0.083	− 0.173	− 3.174
323.15 K							
0.1011	− 0.564	− 0.146	− 0.193	0.191	0.043	− 0.098	− 2.477
0.2059	− 0.923	− 0.214	− 0.308	0.290	0.064	− 0.395	− 4.538
0.3019	− 1.099	− 0.231	− 0.358	0.321	0.059	− 0.576	− 5.926
0.3937	− 1.158	− 0.222	− 0.369	0.314	0.037	− 0.476	− 6.779
0.5023	− 1.121	− 0.192	− 0.343	0.275	− 0.004	− 0.635	− 7.168
0.5840	− 1.028	− 0.161	− 0.304	0.232	− 0.039	− 0.380	− 7.007
0.6946	− 0.835	− 0.114	− 0.232	0.165	− 0.079	− 0.534	− 6.159
0.7788	− 0.644	− 0.078	− 0.168	0.113	− 0.094	− 0.441	− 5.023
0.8707	− 0.398	− 0.041	− 0.095	0.059	− 0.084	− 0.168	− 3.295

Standard uncertainty $s(T) = \pm 0.01$ K, $s(x) = \pm 1.0 \times 10^{-4}$, $s(\rho) = \pm 0.8$ kg m^{-3}, $s(u) = \pm 1$ m s^{-1}, $s(n_D) = \pm 0.0005$, $s(T)$ for n_D = ± 0.02 K, $s(p) = \pm 1.0$ kPa

The deviation of V_m^E, κ_s^E, $K_{s,m}^E$, u^E and ΔR_m with mole fraction of [Bmim][PF_6] and temperature for the studied binary mixtures along with smoothed R–K equation values (Table 4) are graphically depicted in Figs. 2, 4–7 at T/K = 298.15–323.15, respectively.

It has been stated [37–40] that V_m^E and κ_s^E values of the binary mixtures result from the contributions due to the physical, chemical and structural characteristics of the component liquids. The physical contributions comprise dispersion forces and non-specific physical (weak) interactions, which lead to positive V_m^E and κ_s^E values. The chemical contributions involve breaking up the associates present in the pure liquids, resulting in positive V_m^E and values. These contributions also involve specific interactions such as formation of H-bonding, charge transfer (donor–acceptor) complexes, and ion–dipole interactions between the component molecules of the mixture, resulting in negative V_m^E and κ_s^E values. The structural contributions are due to the geometrical fitting (favourable/unfavourable) of the molecules of very different molecular sizes into each other's structures resulting in negative or positive V_m^E and κ_s^E values.

Instead of our craving, the negative V_m^E values suggest the formation of strong ion–dipole interactions between ions formed by ionic liquid [$Bmim^+$] and [PF_6^-] and dipoles of NVP molecules. In this present binary system, the structural contributions are predominant. The composition and temperature dependence of V_m^E for the studied mixtures may be explained based on structural contributions arising from interstitial accommodation and changes of free volume. Another source of negative contribution to V_m^E may be from the fitting of small NVP molecules (molar volume: NVP = 106.93 cm^3 mol^{-1} at T = 298.15 K) into the voids present in bigger [Bmim][PF_6] molecules (molar volumes = 207.85 cm^3 mol^{-1} at T = 298.15 K). Contributions emerging from the geometrical fitting of smaller molecules into the voids accessible in the structure of bigger molecules were likewise considered by others [40, 41] for translating negative V_m^E values for binary mixtures that contains molecules of different molecular sizes. Therefore, the geometrical impact due to interstitial fitting of NVP molecules in the interstices of ionic liquids, and the ion–dipole interactions between highly polar NVP molecules and imidazolium ring of the ionic liquids contributes to the negative values of V_m^E [42, 43].

There is a systematic decrease in V_m^E for all the systems with the rise in temperature. A comparison of the data at different temperatures reveals that the temperature coefficient

$$\left(\partial V_m^E / \partial T\right)_p$$

is negative, indicating that there is a formation of associated species between [Bmim][PF_6] + NVP mixture with a rise in temperature, which results in a contraction in volume of the mixture and hence negative V_m^E values.

We graphically compared our V_m^E results with the mixtures of 1-butyl-3-methylimidazolium with different anions BF_4 [9], PF_6 and NTf_2 [10] in Fig. 3 at 298.15 K. The degree of their influence depends on the nature of anion and cation of the ionic liquids, and the nature of the organic compounds. This suggests that the strength of interactions in these mixtures follows the sequence of [Bmim][PF_6] > [Bmim][BF_4] > [Bmim][NTf_2].

Table 4 Coefficients A_i of Eq. (10) along with standard deviations σ of binary mixture properties

T/K	A_1	A_2	σ	SE	F-value	p value
V_m^E 10^6 m^3 mol^{-1}						
298.15	− 3.787	1.302	0.353	0.013	13,772.50	7.11×10^{-15}
303.15	− 3.935	1.367	0.367	0.014	13,769.49	7.11×10^{-15}
308.15	− 4.088	1.433	0.381	0.015	13,980.95	6.69×10^{-15}
313.15	− 4.250	1.502	0.396	0.015	13,410.77	7.91×10^{-15}
318.15	− 4.391	1.569	0.410	0.016	12,642.82	1.00×10^{-14}
323.15	− 4.563	1.649	0.426	0.017	12,349.60	1.10×10^{-14}
κ_s^E 10^{10} m^2 N^{-1}						
298.15	− 0.591	0.563	0.064	0.008	1182.19	1.29×10^{-10}
303.15	− 0.635	0.592	0.068	0.008	1219.77	1.14×10^{-10}
308.15	− 0.677	0.624	0.073	0.008	1251.73	1.03×10^{-10}
313.15	− 0.718	0.657	0.077	0.009	1256.32	1.01×10^{-10}
318.15	− 0.764	0.694	0.082	0.009	1265.00	9.87×10^{-11}
323.15	− 0.812	0.735	0.087	0.010	1266.58	9.82×10^{-11}
$K_{s,m}^E$ 10^{14} m^5 N^{-1} mol^{-1}						
298.15	− 0.998	0.603	0.099	0.003	20,593.72	1.42×10^{-15}
303.15	− 1.076	0.630	0.106	0.003	20,283.25	1.51×10^{-15}
308.15	− 1.151	0.665	0.113	0.003	20,446.22	1.46×10^{-15}
313.15	− 1.225	0.702	0.120	0.004	19,676.84	1.71×10^{-15}
318.15	− 1.307	0.743	0.128	0.004	19,239.39	1.87×10^{-15}
323.15	− 1.394	0.791	0.137	0.004	18,695.73	2.09×10^{-15}
u^E 10^2 m s^{-1}						
298.15	0.979	− 0.924	0.107	0.010	1814.67	2.34×10^{-11}
303.15	1.020	− 0.928	0.110	0.010	2016.31	1.54×10^{-11}
308.15	1.054	− 0.936	0.113	0.010	2201.12	1.08×10^{-11}
313.15	1.080	− 0.942	0.115	0.010	2388.76	7.81×10^{-12}
318.15	1.113	− 0.953	0.118	0.009	2601.76	5.55×10^{-12}
323.15	1.144	− 0.967	0.121	0.009	2812.94	4.07×10^{-12}
ΔR_m 10^6 m^3 mol^{-1}						
298.15	0.076	− 1.027	0.072	0.006	636.98	1.52×10^{-09}
303.15	0.041	− 0.991	0.070	0.007	553.63	2.65×10^{-09}
308.15	0.019	− 0.951	0.067	0.007	475.89	4.83×10^{-09}
313.15	0.007	− 0.905	0.064	0.007	401.49	9.47×10^{-09}
318.15	− 0.012	− 0.866	0.061	0.007	339.15	1.85×10^{-09}
323.15	− 0.046	− 0.825	0.058	0.008	293.19	3.28×10^{-09}
n_D^E 10^2						
298.15	− 24.141	− 0.527	2.224	0.010	636.98	1.52×10^{-09}
303.15	− 24.999	− 0.652	2.304	0.012	553.63	2.65×10^{-09}
308.15	− 25.881	− 0.765	2.386	0.013	475.89	4.83×10^{-09}
313.15	− 26.803	− 0.888	2.471	0.015	401.49	9.47×10^{-09}
318.15	− 27.603	− 1.036	2.546	0.017	339.15	1.85×10^{-08}
323.15	− 28.585	− 1.203	2.638	0.019	293.19	3.28×10^{-08}

An ultrasonic study is one of the best tools to understand the nature of interactions between solute–solute and solute–solvent or solvent–solvent in the mixture [44]. Nonlinear variation of κ_s^E and $K_{s,m}^E$ as a function of [Bmim][PF_6] of the liquid mixture is sufficient evidence for the existence of molecular interactions in solutions. A perusal of Figs. 4 and 5 also shows that κ_s^E and $K_{s,m}^E$ values become more negative as the temperature is increased from 298.15 to 323.15 K. With the increase in temperature, the kinetic energy of the molecules increases, and a large number of free NVP molecules would be available in the mixture due to breaking of hydrogen bonds and move

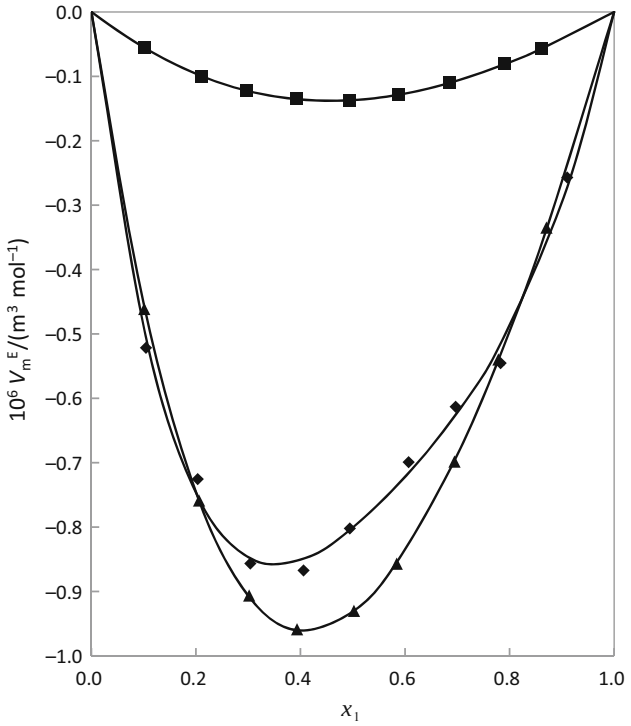

Fig. 3 Comparative excess molar volume of NVP for [BMIM][NTf2] (■); [BMIM][BF_4] (◆); [BMIM][PF6] (▲) at *T*/K = 298.15

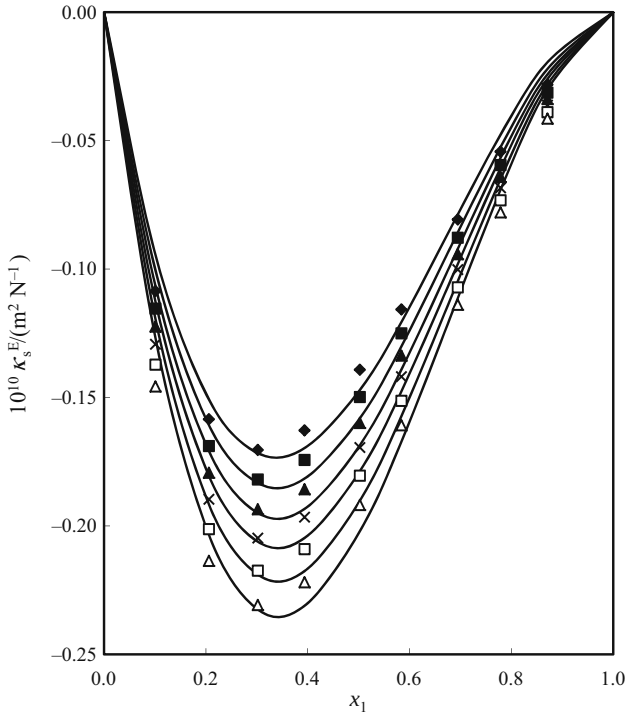

Fig. 4 Plots of excess molar compressibility, κ_s^E versus mole fraction, x_1 of [Bmim][PF_6] for [Bmim][PF_6] + NVP binary mixtures at temperatures, *T*/K = 298.15, ◆; At *T*/K = 303.15, ■; *T*/K = 308.15, ▲; *T*/K = 313.15, ×; *T*/K = 318.15, □; *T*/K = 323.15, Δ. The points represent experimental values, and lines represent values calculated from Eq. (10) using the coefficients given in Table 4

towards C_2 atom of imidazolium ring due to completely dissociated ionic liquid at higher temperature. Therefore, at higher temperature the ion–dipole interactions between unlike molecules (ions from ionic liquid and dipoles of NVP) become more significant due to availability of greater number of amide dipoles, leading to the contraction in volume, thereby decreasing the volume and compressibility of the mixture. This may be explained as follows:

The one kind of properties of imidazolium cations is established in the electrostatic attraction of the aromatic cations. The electrostatic fascination of these salts contains delocalized 3-centre-4-electron configuration across the N_1–C_2–N_3 moiety, a twofold bond between C_4 and C_5 at the inverse side of the ring and a powerless delocalization in the central region [45]. The hydrogen radicals C_2–H, C_4–H, and C_5–H convey nearly a similar charge, yet carbon C_2 is decidedly charged inferable from the electron deficiency in the C=N bond, whereas C_4 and C_5 are practically neutral. The subsequent causticity of the hydrogen atoms is the key tip to comprehend the properties of these ionic liquids. The hydrogen on the C_2 carbon (C_2–H) has been appeared to cling particularly with the solute molecules [46, 47]. It appears to be that the hydrogen atom at C_2 (between nitrogen atoms) can be viewed as acidic to shape a strong hydrogen bond with oxygen atom of NVP. This presumption has been affirmed by Crosthwaite et al. [48].

As expected, the u^E exhibit positive values in the binary mixture at the investigated temperature range. In general, positive deviations in u^E indicate the presence of significant interactions and negative deviations in u^E indicate weak interactions between the unlike molecules in the mixtures [49, 50]. The positive u^E values suggest the formation of significant ion–dipole interactions between the ions [$Bmim^+$] and [PF_6^-] formed by ionic liquid and dipoles of NVP molecules. At higher mole fractions ($x_1 > 0.9$), the interactions between like molecules IL–IL and NVP–NVP seem dominating in these binary mixtures. The observed positive values of u^E for these binary mixtures indicate strong interactions involving the formation of ion–dipole and hydrogen bonding between the component molecules of the mixture. Thus, the trends of u^E versus x_1 (Fig. 6) strongly support the behaviour of V_m^E and κ_s^E for these mixtures.

The results presented in Fig. 5S indicate that $\Delta_\phi n_D$ values are negative for these mixtures over the entire mole fraction range at all investigated temperatures. In general, the positive deviations in Δn values (on volume fraction dependence basis) are considered due to the presence of

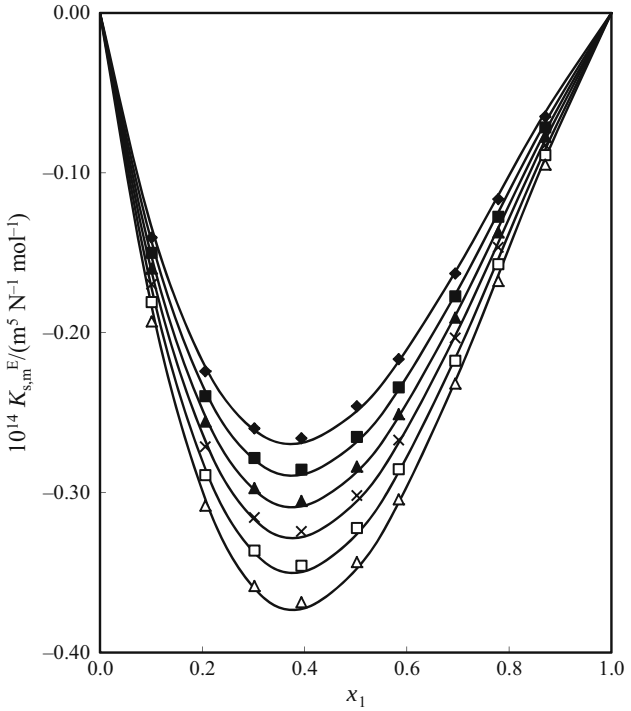

Fig. 5 Excess molar isentropic compressibilities $K^{E}_{s,m}$ versus mole fraction, x_1 of [Bmim][PF_6] for [Bmim][PF_6] + NVP binary mixtures at temperatures, T/K = 298.15, ◆; At T/K = 303.15, ■; T/K = 308.15, ▲; T/K = 313.15, ×; T/K = 318.15, □; T/K = 323.15, Δ. The points represent experimental values, and lines represent values calculated from Eq. (10) using the coefficients given in Table 4

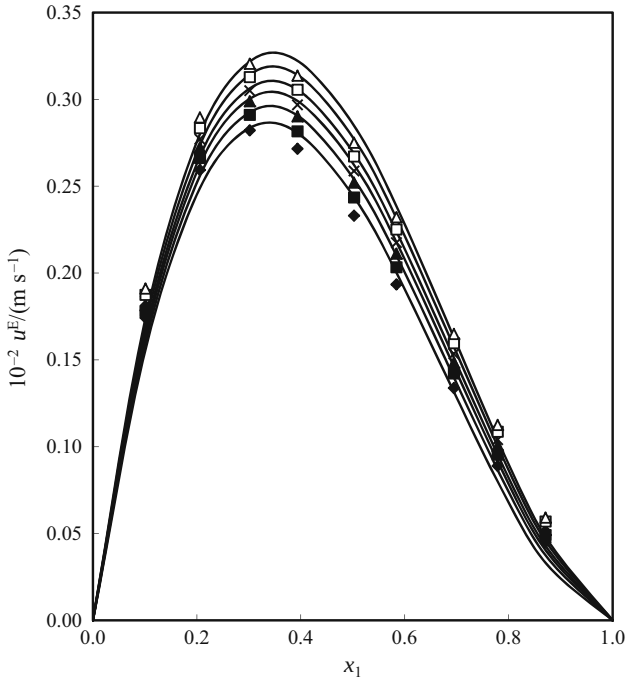

Fig. 6 Excess speed of sound u^{E} versus mole fraction, x_1 of [Bmim][PF_6] for [Bmim][PF_6] + NVP binary mixtures at temperatures, T/K = 298.15, ◆; At T/K = 303.15, ■; T/K = 308.15, ▲; T/K = 313.15, ×; T/K = 318.15, □; T/K = 323.15, Δ. The points represent experimental values, and lines represent values calculated from Eq. (10) using the coefficients given in Table 4

significant interactions in the mixtures, whereas negative deviations in $\Delta_{\phi}n_D$ values indicate weak interactions between the components of the mixture [51]. The $\Delta_{\phi}n_D$ values decrease with the increase in temperature for each binary mixture, indicating that the ion–dipole interactions between unlike molecules decrease due to less availability of NVP dipoles.

The outcomes introduced in Fig. 7 demonstrate that ΔR_m values likewise show sigmoid pattern with positive ΔR_m values at low mole parts ($x_1 < 0.5$) of [Bmim][PF_6] and negative ΔR_m values at higher mole parts ($x_1 > 0.5$) of [Bmim][PF_6] in these binary mixtures at each examined temperature. Positive values of ΔR_M indicate strong intermolecular interactions, while negative values indicate weak intermolecular interactions (dispersion forces/ion–dipole interactions). All in all, the positive deviations in ΔR_m values (on volume part reliance premise) are considered because of nearness of huge communications in the mixtures, though negative deviations in ΔR_m values indicate frail collaborations between the segments of the mixture [30, 51]. The ΔR_m values increase with the increase in temperature for this binary mixture, demonstrating that the ion–dipole interactions between dissimilar molecules increase because of accessibility of more NVP dipoles on softening of affiliations present in ideal NVP.

A comparison of isobaric thermal expansivity (α_p) data in Table 2S with reported values reveals a fairly consistent between the two, and the AAD between both was ± 0.4% for IL and NVP is ± 0.1% which can be considered quite acceptable. Thus, the density data were precise enough to allow the accurate determination of the temperature dependence of α_p for liquids using the incremental method. Here in our case the density values are linearly decrement w.r.t temperature. Figure 6S shows the α^{E}_{p} values obtained against composition; it is clearly observed that mixtures exhibit relatively small or negligible change in this excess quantity.

Partial molar quantities

A perusal of Figs. 8 and 9 (Supplementary material Tables 3S & 4S) indicates that the values of $\overline{V}^{E}_{m,1}$ and $\overline{V}^{E}_{m,2}$; $\overline{K}^{E}_{s,m,1}$ and $\overline{K}^{E}_{s,m,2}$ are negative for both the binary mixtures over the whole composition range. This suggests that the molar volumes (or) molar isentropic compressibilities of

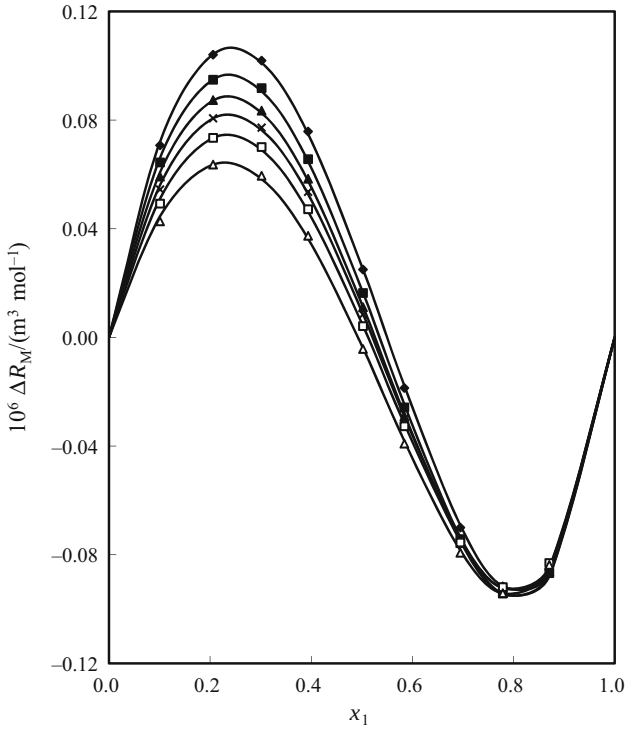

Fig. 7 Deviation in molar refraction ΔR_M versus mole fraction, x_1 of [Bmim][NTf_2] for [Bmim][NTf_2] + NVP binary mixtures at temperatures, T/K = 298.15, ◆; At T/K = 303.15, ■; T/K = 308.15, ▲; T/K = 313.15, ×; T/K = 318.15, □; T/K = 323.15, Δ. The points represent experimental values, and lines represent values calculated from Eq. (10) using the coefficients given in Table 4

each component in the mixture are less than their respective molar volume (or) molar isentropic compressibilities in the pure state, *i.e.* there is a decrease in the volume (or) isentropic compressibilities on mixing [Bmim][PF_6] with NVP. In general, the negative $\overline{V}^{E}_{m,1}$ and $\overline{V}^{E}_{m,2}$; $\overline{K}^{E}_{s,m,1}$ and $\overline{K}^{E}_{s,m,2}$ values indicate the presence of significant solute–solvent interactions between unlike molecules, whereas the positive $\overline{V}^{E}_{m,1}$ and $\overline{V}^{E}_{m,2}$; $\overline{K}^{E}_{s,m,1}$ and $\overline{K}^{E}_{s,m,2}$ values indicate the presence of weak interactions [52] in the mixture. The observed negative $\overline{V}^{E}_{m,1}$ and $\overline{V}^{E}_{m,2}$; $\overline{K}^{E}_{s,m,1}$ and $\overline{K}^{E}_{s,m,2}$ values indicate that [Bmim][PF_6] − NVP interactions are stronger than interactions between like molecules which lead to decrease in volume and compressibility.

A look at Tables 5 and 6 indicates that the values of $\overline{V}^{\circ E}_{m,1}$ and $\overline{V}^{\circ E}_{m,2}$; $\overline{K}^{\circ E}_{s,m,1}$ and $\overline{K}^{\circ E}_{s,m,2}$ are negative for these binary systems at each investigated temperature. This suggests that the V_m or $K_{s,m}$ of each component in the mixture is less than their respective V_m or $K_{s,m}$ in the pure state, *i.e.* there is a contraction in volume or decrease in the $K_{s,m}$ on mixing [Bmim][PF_6] with NVP. The observed negative $\overline{V}^{\circ E}_{m,1}$ and $\overline{V}^{\circ E}_{m,2}$ values indicate that [Bmim][PF_6]–

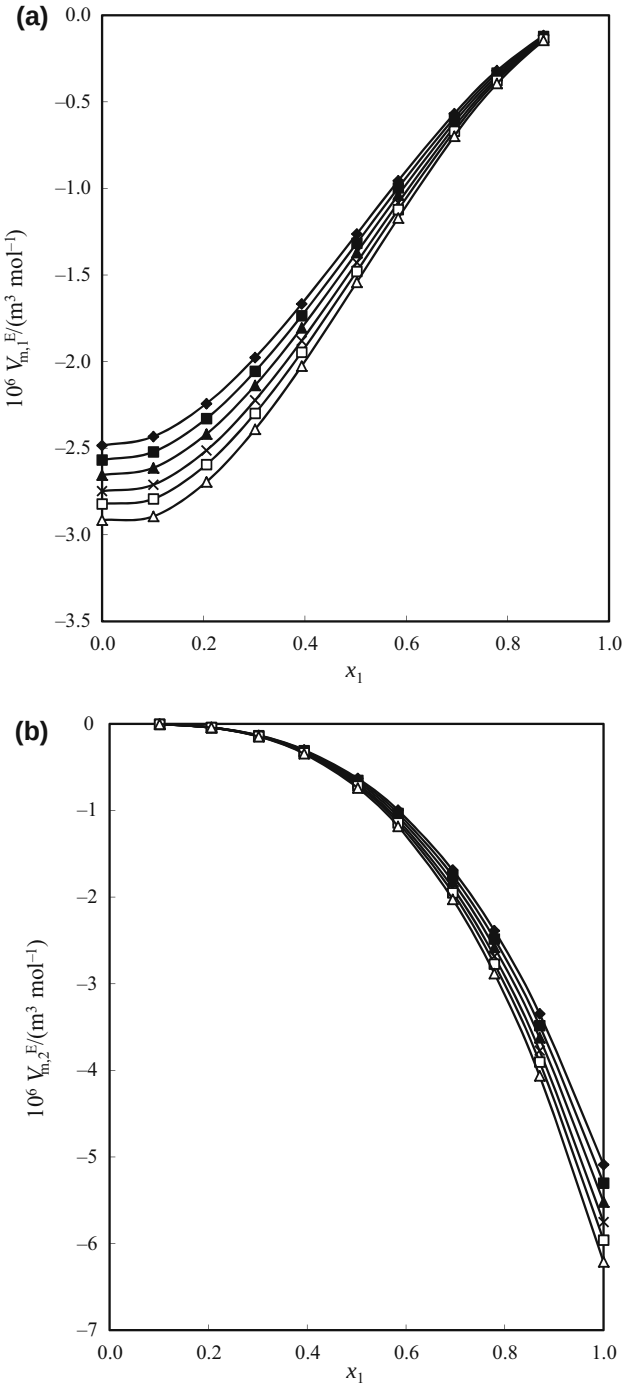

Fig. 8 Variation of excess partial molar volumes, $\overline{V}^{E}_{m,1}$ and $\overline{V}^{E}_{m,2}$ of **a** [Bmim][PF_6] and **b** NVP, respectively, of against mole fraction, x_1 of [Bmim][PF_6] for the binary mixtures at temperatures, T/K = 298.15, ◆; At T/K = 303.15, ■; T/K = 308.15, ▲; T/K = 313.15, ×; T/K = 318.15, □; T/K = 323.15, Δ

NVP interactions are stronger than interactions between like molecules.

The values of $\overline{V}^{\circ E}_{m,1}$ and $\overline{V}^{\circ E}_{m,2}$; $\overline{K}^{\circ E}_{s,m,1}$ and $\overline{K}^{\circ E}_{s,m,2}$ can be analysed in terms of structural and geometrical compressibility as suggested by Hall and others [52–54]. The

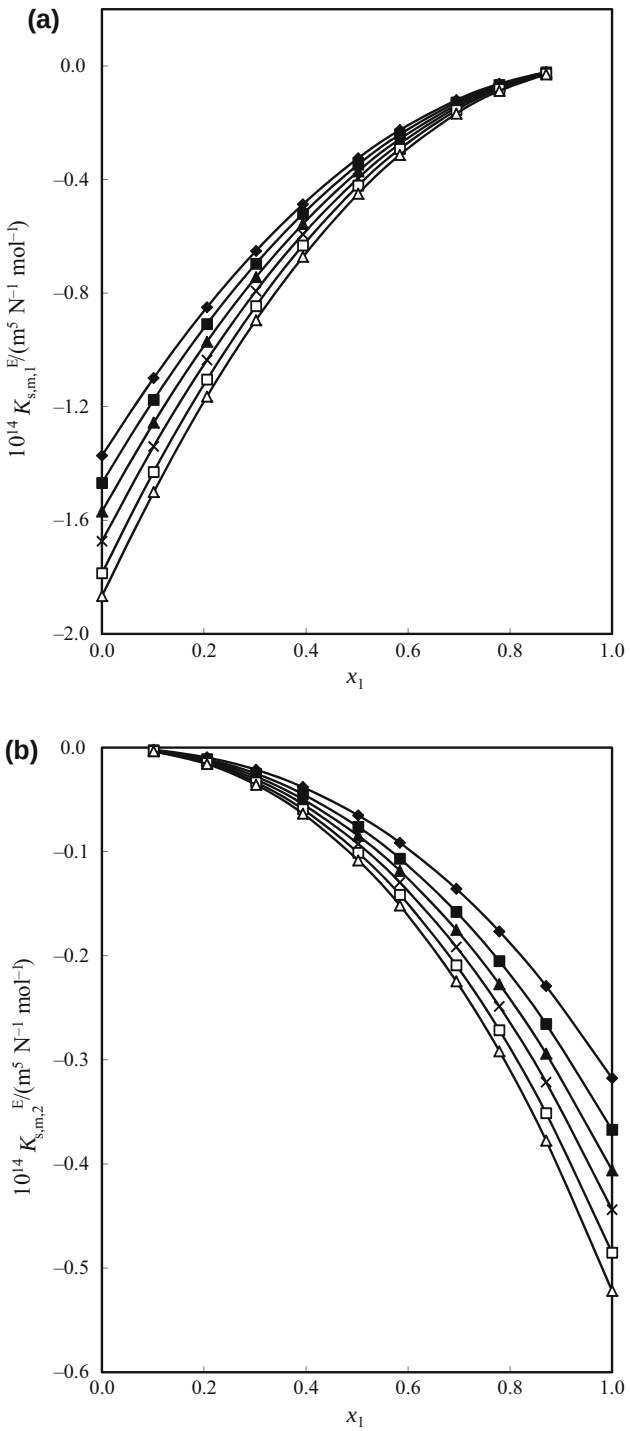

Fig. 9 Variation of excess partial molar isentropic compressibilities, $\overline{K}^{E}_{s,m,1}$ and $\overline{K}^{E}_{s,m,2}$ of (a) [Bmim][NTf_2] and (b) NVP, respectively, of against mole fraction, x_1 of [Bmim][NTf_2] for the binary mixtures at temperatures, T/K = 298.15, ◆; At T/K = 303.15, ■; T/K = 308.15, ▲; T/K = 313.15, ×; T/K = 318.15, □; T/K = 323.15, Δ

structural compressibility results from the breakdown of associated structure (on mixing [Bmim][PF_6] with NVP), whereas geometrical compressibility is due to the simultaneous compression of the molecules (due to specific interactions between [Bmim][PF_6] and NVP molecules) leading to contraction in volume and decrease in compressibility. The observed values of $\overline{V}^{\circ E}_{m,1}$ and $\overline{V}^{\circ E}_{m,2}$; $\overline{K}^{\circ E}_{s,m,1}$ and $\overline{K}^{\circ E}_{s,m,2}$ indicate that the geometrical compressibility factor dominates in these mixtures. Also, $\overline{V}^{\circ E}_{m,1}$ and $\overline{V}^{\circ E}_{m,2}$; $\overline{K}^{\circ E}_{s,m,1}$ and $\overline{K}^{\circ E}_{s,m,2}$ values decrease with the increase in temperature (Tables 5 and 6) for each binary mixture which further supports the trends observed in V^{E}_{m} and κ^{E}_{s} values.

Prediction of refractive index using mixing rules

Refractive index of liquid mixtures is an important property for structural characterization, engineering calculations and assessing purity of substance. The refractive index is used in the continuum model of matter and parameterizes how matter interacts with electromagnetic polarizability (Kier and Hall) to estimate the boiling point with Meissner's method or to estimate the other thermodynamic properties. Measurement of refractive index can be used for providing information about the forces between the molecules [55] or their behaviour when they are in solution [56]. The refractive indices of the binary mixtures have been theoretically calculated from the refractive index data of pure components of the mixtures using nine mixing rules [39]. There exist the definite expansion and/or contraction of liquid when the mixing takes place and also densities become changed, and due to this density change, we observe a considerable variation in refractive index. This was firstly examined by Laplace and later by Gladstone–Dale who gave a formula for the determination of refractive index of a liquid mixture by using the properties of their pure components and has been used for optical analysis (determination of composition), or to calculate the density of a liquid for use in fluid dynamics such as flow visualization. We have various empirical and semi-empirical relations that have been formulated in this connection, and it is found out that rules due to Lorentz–Lorentz and Weiner are extensively used. It is important to mention that there exists a drawback of these mixing rules in their inability to account for changes in volume and refractivity during mixing; this is because of volume additivity. In the light of above description, it is fully feasible to make discussion for these mixing rules for the mixtures taken in this study. The values are seen to decrease with the increase in temperature for pure components as well as mixtures, but the AAPD values tend to increase with temperature which can be accounted by the changing density and nonlinear

Table 5 Values $\bar{V}^{\circ}_{m,1}, \bar{V}^{*}_{m,1}, \bar{V}^{\circ E}_{m,1}, \bar{V}^{\circ}_{m,2}, \bar{V}^{*}_{m,2}, \bar{V}^{\circ E}_{m,2}$ of the components for [Bmim] [PF_6] + NVP at temperatures T = 298.15–323.15 K

T/K	$10^6 \bar{V}^{\circ}_{m,1}$ m^3 mol^{-1}	$10^6 \bar{V}^{*}_{m,1}$	$10^6 \bar{V}^{\circ E}_{m,1}$	$10^6 \bar{V}^{\circ}_{m,2}$	$10^6 \bar{V}^{*}_{m,2}$	$10^6 \bar{V}^{\circ E}_{m,2}$
298.15	304.24	306.73	− 2.48	101.84	106.93	− 5.09
303.15	305.12	307.69	− 2.57	102.08	107.39	− 5.30
308.15	305.99	308.65	− 2.66	102.32	107.85	− 5.52
313.15	306.87	309.62	− 2.75	102.56	108.31	− 5.75
318.15	307.77	310.60	− 2.82	102.82	108.78	− 5.96
323.15	308.66	311.58	− 2.91	103.04	109.25	− 6.21

Table 6 Values $\overline{K}^{\circ}_{s,m,1}, K^{*}_{s,m,1}, \overline{K}^{\circ E}_{s,m,1}, \overline{K}^{\circ}_{s,m,2}, K^{*}_{s,m,2}$ and $\overline{K}^{\circ E}_{s,m,2}$ of the components for [Bmim] [PF_6] + NVP at temperatures T = 298.15–323.15 K

T/K	$10^{14}.\overline{K}^{\circ}_{s,m,1}$ (m^5 N^{-1} mol^{-1})	$10^{14}.K^{*}_{s,m,1}$	$10^{14}.\overline{K}^{\circ E}_{s,m,1}$	$10^{14}.\overline{K}^{\circ}_{s,m,2}$	$10^{14}.K^{*}_{s,m,2}$	$10^{14}.\overline{K}^{\circ E}_{s,m,2}$
298.15	5.917	7.289	− 1.373	4.122	4.439	− 0.318
303.15	5.990	7.458	− 1.468	4.223	4.590	− 0.367
308.15	6.062	7.631	− 1.569	4.340	4.747	− 0.406
313.15	6.131	7.805	− 1.674	4.466	4.910	− 0.444
318.15	6.196	7.983	− 1.787	4.594	5.079	− 0.485
323.15	6.296	8.163	− 1.867	4.734	5.256	− 0.522

Table 7 Average percentage deviations (APDs) in theoretically calculated refractive indices by using Arago–Biot (A–B), Gladstone–Dale (G–D), Newton (N), Eyring and John (E–J), Lorentz–Lorentz (L–L), Heller (H), Eykman (EK), Oster (OS), and Weiner (W) relations for [Bmim][Pf_6] + NVP binary mixtures at temperatures T/K = 298.15–323.15

T/K	Average percentage deviations (APDs)								
	A–B	G–D	N	E–J	L–L	H	EK	OS	W
298.15	0.151	0.151	0.117	0.170	0.192	0.184	0.247	0.274	0.166
303.15	0.151	0.151	0.117	0.170	0.192	0.183	0.246	0.272	0.166
308.15	0.153	0.153	0.118	0.172	0.193	0.184	0.247	0.273	0.168
313.15	0.156	0.156	0.121	0.175	0.197	0.187	0.249	0.275	0.171
318.15	0.158	0.158	0.123	0.176	0.198	0.188	0.250	0.275	0.172
323.15	0.158	0.158	0.123	0.177	0.198	0.189	0.250	0.274	0.173

behaviour between molecules as reflected by refractive index evaluation [57]. Among all equations proposed to estimate the refractive index of the mixtures from the pure components, Newton relation was found best other than equations. APD of the mixture at all studied temperatures is summarized in Table 7 and follows the sequence Oster > Eykman > Lorentz–Lorenz > Heller > Eyring and John > Weiner > Arago–Biot ≥ Gladstone–Dale > Newton.

FTIR analysis

The nature and degree of collaborations between the ILs and natural solvents are all around reported through thermodynamic reviews and are not adequate to determine the correct way of solute-dissolvable communications between the connecting segments. To accomplish this objective, here we analysed the intermolecular interactions between the ionic liquid [Bmim][PF_6] and NVP at atomic level over the entire creation extend utilizing FTIR spectroscopy. It is an important tool for recognizable of little change in dipole moments.

The infrared spectra for pure [Bmim][PF_6], NVP and their binary mixtures are shown in Fig. 7S (*Supplementary material*) and are summarized in Table 8. In 1-butyl-3-methylimidazolium cation, the CH stretching region between 2800 and 3200 cm^{-1} was analysed. For [Bmim][PF_6], the signals in this region can be split into two parts: (1) the signals between 2800 and 3000 cm^{-1} result from aliphatic CH groups in the butyl and methyl moieties, (2) signals between 3000 and 3200 cm^{-1} can be assigned to CH modes predominantly originating from the aromatic imidazolium ring, from C_2–H and $C_{4,5}$–H stretching

Table 8 Infrared transmittance wave numbers between [Bmim][Pf_6] in NVP at room temperature and atmospheric pressure P = 0.1 MPa

IL	NVP	C–H	C_2–H	$C_{4,5}$–H	C=O	C=N	P–F
0.0000	1.0000	–	3109.6	–	1692.9	–	–
0.1011	0.8989	2961.6	3111.0	3156.3	1690.1	623.3	745.1
0.2059	0.7941	2962.3	3112.4	3157.8	1688.7	623.3	748.0
0.3019	0.6981	2962.3	3115.3	3162.0	1688.7	623.3	748.0
0.3937	0.6063	2963.7	3118.1	3164.8	1690.1	621.9	748.7
0.5023	0.4977	2963.7	3120.9	3166.3	1690.1	621.9	748.7
0.5840	0.4160	2963.7	3122.3	3166.3	1691.5	621.9	748.7
0.6946	0.3054	2965.1	3123.8	3167.7	1692.9	621.9	748.7
0.7788	0.2212	2965.1	3124.2	3169.1	1692.9	621.9	748.7
0.8707	0.1293	2965.1	3124.8	3170.5	1692.9	621.9	749.4
1.0000	0.0000	2966.5	3126.6	3170.5	–	621.9	749.4

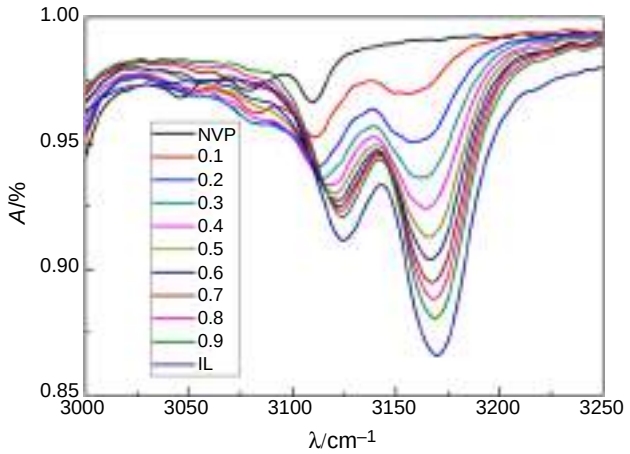

Fig. 10 IR spectra for [Bmim][PF_6] + NVP mixtures in the range of 3000–3250 cm^{-1}

frequencies. The C_2–H vibrational frequency (3124.7 cm^{-1}) is shifted by about 44.8 cm^{-1} to lower frequencies than the C_4–H and C_5–H stretches (3169.5 cm^{-1}) due to its stronger acidic character. The pure liquid NVP has two very strong vibration bands in the IR spectrum at 1629 and 1692.9 cm^{-1} corresponding to C=C and C=O stretching frequencies, respectively. There is a possibility for conjugation of olefinic group with the carbonyl group through electron pair of the nitrogen. Due to the resonance system involving five atoms, C=C and C=O stretching frequencies are inter dependable.

In the present mixture, observable changes were noticed between the frequencies of 3000–3200 cm^{-1} which belong to C_2–H and $C_{4,5}$–H stretching frequencies of imidazolium cation as well as C=O and C=C stretching frequencies of NVP. As mole fraction of NVP increases, a blue shift in C_2–H and $C_{4,5}$–H stretching frequencies indicates the

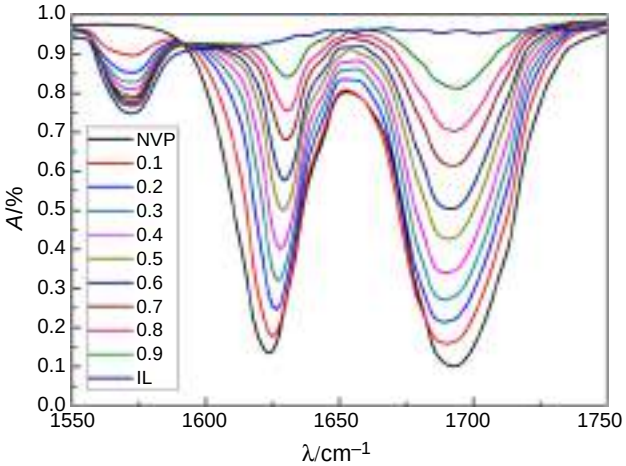

Fig. 11 IR spectra for [Bmim][PF_6] + NVP mixtures in the range of 1550–1750 cm^{-1}

formation of hydrogen bond between $[Bmim]^+$ and NVP as C_2–H and $C_{4,5}$–H experience weak hydrogen bonding interactions than in pure [Bmim][PF_6]. The blue shift is very predominant in C_2–H frequencies when compared to $C_{4,5}$–H stretching frequencies which indicates that more acidic C_2–H plays a major role in the formation of hydrogen bond with carbonyl oxygen of NVP (Fig. 10). Simultaneously, as mole fraction of IL increases a clear red shift in C=O and C=C Sym stretch frequencies are observed in NVP. This clearly indicates the formation of intermolecular hydrogen bond between hydrogen of aromatic imidazolium ring and carbonyl oxygen of NVP (Fig. 11). Ion–dipole interactions can also explain on the basis of anion $[PF_6]^-$ with NVP. A blue shift was observed in P-F of [PF_6]–anion by the addition of NVP.

Conclusions

The present study reported the densities, ρ, speeds of sound, u and refractive indices, n_D of the binary mixtures of [Bmim][PF_6] with NVP over whole composition range at different temperatures. From the experimental data, various physicochemical parameters, viz. V_m^E, κ_s^E, u^E, $K_{s,m}^E$ and $\Delta_\phi n_D$ of the mixtures; $\bar{V}_{m,1}$ and $\bar{V}_{m,2}$, $\bar{K}_{s,m,1}$ and $\bar{K}_{s,m,2}$, $\bar{V}_{m,1}^E$ and $\bar{V}_{m,2}^E$ and $\bar{K}_{s,m,1}^E$ and $\bar{K}_{s,m,2}^E$ over whole composition range; $\bar{V}_{m,1}^\circ$ and $\bar{V}_{m,2}^\circ$; $\bar{K}_{s,m,1}^\circ$ and $\bar{K}_{s,m,2}^\circ$; $\bar{V}_{m,1}^{\circ E}$ and $\bar{V}_{m,2}^{\circ E}$ and $\bar{K}_{s,m,1}^{\circ E}$ and $\bar{K}_{s,m,2}^{\circ E}$ of the components infinite dilution have been calculated. The results have been discussed in terms of intermolecular interactions in these mixtures. The results indicate the formation of strong ion–dipole interactions between ionic liquid [Bmim][PF_6] and NVP molecules and the geometrical effect due to interstitial fitting of smaller NVP molecules into the interstices of ionic liquid

molecules. The FTIR spectra of these mixtures have also been recorded at 298.15 K and analysed in terms of intermolecular interactions. FTIR spectra results further supported the above conclusions regarding interactions in these mixtures. The V_m^E values for these mixtures are predicted well by PFP theory. The refractive index data are well correlated by various mixing rules. All the equations used for predicting refractive index exhibit excellent agreement and generate AAPD values much below 1%. The strength of interactions of 1-butyl-3-methylimidazolium with different anions follows the sequence of $[Bmim][PF_6] > [Bmim][BF_4] > [Bmim][NTf_2]$.

Acknowledgements P. Suneetha was thankful to the CSIR, India, for the award of Senior Research Fellowship. The authors were also thankful to Arvind kumar, Principal Scientist, CSMCRI, India, for providing the research facilities.

Compliance with ethical standards

Conflict of interest The authors declare no competing financial interest.

References

1. Iloukhani H, Samiey B, Moghaddasi MA. Speeds of sound, isentropic compressibilities, viscosities and excess molar volumes of binary mixtures of methylcyclohexane + 2-alkanols or ethanol at T = 298.15 K. J Chem Thermodyn. 2006;38:190–200.
2. Tome LI, Carvalho PJ, Freire MG, Marrucho IM, Fonseca IM, Ferreira AG, Coutinho JA, Gardas RL. Measurements and correlation of high-pressure densities of imidazolium-based ionic liquids. J Chem Eng Data. 2008;53:1914–21.
3. Korokin A (ed). Ionic liquids: theory, properties, new approaches. Rijeka: InTech (2011). http://www.intechopen.com/books/ionic-liquids-theory-properties-new-approaches. Accessed 28 Feb 2011.
4. Ishikawa M, Sugimoto T, Kikuta M, Ishiko E, Kono M. Pure ionic liquid electrolytes compatible with a graphitized carbon negative electrode in rechargeable lithium-ion batteries. J Power Sources. 2006;162:658–62.
5. Hallett JP, Welton T. Room-temperature ionic liquids: solvents for synthesis and catalysis. 2. Chem Rev. 2001;11:3508–76.
6. Wasserscheid P, Welton T, editors. Ionic liquids in synthesis. New York: Wiley-VCH Verlag GmbH; 2008.
7. Anderson JL, Armstrong DW. High-stability Ionic liquids. A new class of Stationary phases for gas chromatography. Anal Chem. 2003;75:4851–8.
8. https://patents.google.com/patent/US2767119A/en, grant dated 16 Oct 1956.
9. Sunkara GR, Tadavarthi MM, Tadekoru VK, Tadikonda SK, Bezawada SR. Density, refractive index, and speed of sound of the binary mixture of 1-butyl-3-methylimidazolium tetrafluoroborate + *N*-vinyl-2-pyrrolidinone from T = (298.15 to 323.15) K at atmospheric pressure. J Chem Eng Data. 2015;60:886–94.
10. Suneetha P, Krishna TS, Gowrisankar M, Ravindhranath K, Ramchandran D. Molecular interaction between binary mixtures 1-butyl-3-methyl-imidazolium bis (trifluoromethylsulfonyl) imide with *N*-vinyl-2-pyrrolidinone at different temperatures. J Chem Thermodyn. 2017;2017(108):181–92.
11. Krishna TS, Narendra K, Sankar MG, Nain AK, Munibhadrayya B. Physicochemical and spectroscopic studies of molecular interactions of 1-butyl-3-methylimidazolium hexafluorophosphate + 2-methoxyethanol or 2-ethoxyethanol binary mixtures at temperatures from 298.15 to 323.15 K. J Mol Liq. 2017;227:333–50.
12. Scholz E. Karl Fischer titration. Berlin: Springer; 1984.
13. Dupont J, Consorti CS, Saurez PAZ, de Souza RF. Preparation of 1-butyl-3-methyl imidazolium-based room temperature ionic liquids. Org Synth. 2002;79:236.
14. Dupont J, Consorti CS, Saurez PAZ, de Souza RF. Org Synth. 2004;10:184.
15. Danten Y, Cabaco MI, Besnard M. Interaction of water highly diluted in 1-alkyl-3-methyl imidazolium ionic liquids with the PF6- and BF4- anions. J Phys Chem A. 2009;113:2873.
16. Talaty ER, Raja S, Storhaug VJ, Dolle A, Carper WR. Raman and infrared spectra and ab initio calculations of C2-4MIM imidazolium hexafluorophosphate ionic liquids. J Phys Chem B. 2004;108:13177.
17. Riddick JA, Bunger WB, Sakano TK. Organic solvents physical properties and methods of purification, vol. II. 4th ed. New York: Wiley Interscience; 1986.
18. Krishna TS, Narendra K, Sankar MG, Nain AK, Munibhadrayya B. Thermodynamic, excess and optical studies on the intermolecular interactions of binary liquid mixtures of imidazolium based ILs. J Chem Thermodyn. 2016;2016(98):262–71.
19. George J, Sastry NV. Densities, viscosities, speeds of sound, and relative permittivities for water + cyclic amides (2-pyrrolidinone, 1-methyl-2-pyrrolidinone, and 1-vinyl-2-pyrrolidinone) at different temperatures. J Chem Eng Data. 2004;49:235–42.
20. Gomes de Azevedo R, Esperança JM, Najdanovic-Visak V, Visak ZP, Guedes HJ, Nunes da Ponte M, Rebelo LP. Thermophysical and thermodynamic properties of 1-butyl-3-methylimidazolium tetrafluoroborate and 1-butyl-3-methylimidazolium hexafluorophosphate over an extended pressure range. J Chem Eng Data. 2005;2005(50):997–1008.
21. Troncoso J, Cerdeirina CA, Sanmamed YA, Romaní L, Rebelo LPN. Thermodynamic properties of imidazolium-based ionic liquids: densities, heat capacities, and enthalpies of fusion of [bmim][PF_6] and [bmim][NTf_2]. J Chem Eng Data. 2006;51:1856–9.
22. Jacquemin J, Ge R, Nancarrow P, Rooney DW, Costa Gomes MF, Padua AA, Hardacre C. Prediction of ionic liquid properties. I. Volumetric properties as a function of temperature at 0.1 MPa. J Chem Eng Data. 2008;53:716–26.
23. Fan W, Zhou Q, Sun J, Zhang S. Density, excess molar volume, and viscosity for the methyl methacrylate + 1-butyl-3-methylimidazolium hexafluorophosphate ionic liquid binary system at atmospheric pressure. J Chem Eng Data. 2009;54:2307–11.
24. Zhong Y, Wang H, Diao K. Densities and excess volumes of binary mixtures of the ionic liquid 1-butyl-3-methylimidazolium hexafluorophosphate with aromatic compound at T = (298.15 to 313.15) K. J Chem Thermodyn. 2007;39:291–6.
25. Pereiro AB, Legido JL, Rodri A. Physical properties of ionic liquids based on 1-alkyl-3-methylimidazolium cation and hexafluorophosphate as anion and temperature dependence. J Chem Thermodyn. 2007;39:1168–75.
26. Geng Y, Chen S, Wang T, Yu D, Peng C, Liu H, Hu Y. Density, viscosity and electrical conductivity of 1-butyl-3-methylimidazolium hexafluorophosphate + monoethanolamine and + *N*,*N*-dimethylethanolamine. J Mol Liq. 2008;143:100–8.
27. Pal A, Kumar B. Volumetric, acoustic and spectroscopic studies for binary mixtures of ionic liquid (1-butyl-3-methylimidazolium

hexafluorophosphate) with alkoxyalkanols at T = (288.15 to 318.15) K. J Mol Liq. 2011;163:128–34.
28. Suneetha P, Krishna TS, Gowrisankar M, Ramachandran D. Volumetric, acoustic and spectroscopic study of 1-butyl-3-methylimidazolium trifluoromethanesulfonate with alkoxyalkanols at different temperatures. J Mol Liq. 2017;238:170–83.
29. Krishna TS, Nain AK, Chentilnath S, Punyaseshudu D, Munibhadrayya B. Densities, ultrasonic speeds, refractive indices, excess and partial molar properties of binary mixtures of imidazolium based ionic liquid with pyrrolidin-2-one at temperatures from 298.15K. J Chem Thermodyn. 2016;101:103–14.
30. Douheret G, Davis MI, Reis JCR, Blandamer MJ. Isentropic compressibilities-experimental origin and the quest for their rigorous estimation in thermodynamically ideal liquid mixtures. Chem Phys Chem. 2001;2:148–61.
31. Douheret G, Davis MI, Reis JCR. Excess isentropic compressibilities and excess ultrasound speeds in binary and ternary liquid mixtures. Fluid Phase Equilib. 2005;231:246–9.
32. Benson GC, Kiyohara O. Evaluation of excess isentropic compressibilities and isochoric heat capacities. J Chem Thermodyn. 1979;11:1061–4.
33. Srinivasu JV, Krishna TS, Narendra K, SrinivasaRao G, SubbaRao B. Elucidation of H-bond and molecular interactions of 1,4-butanediol with cresols: acoustic and volumetric data. J Mol Liq. 2017;236:27–37.
34. Cerdeirina CA, Tovar CA, Lez-Salgado DG, Carballo E, Romanoa L. Isobaric thermal expansivity and thermophysical characterization of liquids and liquid mixtures. Phys Chem Chem Phys. 2001;3:5230–6.
35. Brocos P, Pineiro A, Bravo R, Amigo A. Refractive indices, molar volumes and molar refractions of binary liquid mixtures: concepts and correlations. Phys Chem Chem Phys. 2003;5:550–7.
36. Redlich O, Kister AT. Algebraic representation of thermodynamic properties and the classification of solutions. Ind Eng Chem. 1948;40:345–8.
37. Iloukhani H, Ghorbani R. Volumetric properties of *N*,*N*-dimethylformamide with 1, 2-alkanediols at 20 C. J Sol Chem. 1998;27(2):141–9.
38. Davis MI, Douheret G, Reis JCR, Blandamer MJ. Apparent and partial ideal molar isentropic compressibilities of binary liquid mixtures. Phys Chem Chem Phys. 2001;3:4555–9.
39. Krishna TS, Raju KTSS, Gowrisankar M, Nain AK, Munibhadrayya B. Volumetric, ultrasonic and spectroscopic studies of molecular interactions in binary mixtures of 1-butyl-3-methylimidazolium hexafluorophosphate with 2-propoxyethanol at temperatures from 298.15 to 323.15 K. J Mol Liq. 2016;216:484–95.
40. Ali A, Nain AK. Ultrasonic and volumetric study of binary mixtures of benzyl alcohol with amides. Bull Chem Soc Jpn. 2002;75:681–7.
41. Assarsson P, Eirich FR. Properties of amides in aqueous solution. I. Viscosity and density changes of amide-water systems. An analysis of volume deficiencies of mixtures based on molecular size differences (mixing of hard spheres). J Phys Chem. 1968;72:2710–9.
42. Zafarani-Moattar MT, Shekaari H. Volumetric and speed of sound of ionic liquid, 1-butyl-3-methylimidazolium hexafluorophosphate with acetonitrile and methanol at T = (298.15 to 318.15) K. J Chem Eng Data. 2005;50:1694–9.
43. Wang J, Zhu A, Zhao Y, Zhuo K. Excess molar volumes and excess logarithm viscosities for binary mixtures of the ionic liquid 1-butyl-3-methylimidazolium hexaflurophosphate with some organic compounds. J Solution Chem. 2005;34:585–96.
44. Reddy PM, Venkatesu P. Densities and ultrasonic studies for binary mixtures of tetrahydrofuran with chlorobenzenes, chlorotoluenes and nitrotoluenes at 298.15 K. Fluid Phase Equilib. 2011;310:74–81.
45. Hunt PA, Kirchner B, Welton T. Characterising the electronic structure of ionic liquids: an examination of the 1-butyl-3-methylimidazolium chloride ion pair. J Chem Eur. 2006;12:6762–75.
46. Aggarwal A, Lancaster NL, Sethi AR, Welton T. The role of hydrogen bonding in controlling the selectivity of Diels-Alder reactions in room-temperature ionic liquids. Green Chem. 2002;4:517–20.
47. Znamenskiy V, Kobrak MN. Molecular dynamics study of polarity in room-temperature ionic liquids. J Phys Chem B. 2004;2004(108):1072–9.
48. Crosthwaite JM, Aki SN, Maginn EJ, Brennecke JF. Liquid phase behavior of imidazolium-based ionic liquids with alcohols. J Phys Chem B. 2004;2004(108):5113–9.
49. Kawaizumi F, Ohno M, Miyahara Y. Ultrasonic and volumetric investigation of aqueous solutions of amides. Bull Chem Soc Jpn. 1977;50:2229–36.
50. Prakash O, Sinha S. Ultrasonic studies in binary mixtures of tetrahydrofuran with formamide, methyl formamide, dimethyl formamide and 2-methyl pyridine. Acustica. 1984;54:223–5.
51. Pineiro A, Brocos P, Amigo A, Pintos M, Bravo R. Prediction of excess volumes and excess surface tensions from experimental refractive indices. Phys Chem Liq. 2000;38:251–60.
52. Hall L. The origin of ultrasonic absorption in water. Phys Rev. 1948;73:775–84.
53. Hawrylak B, Gracie K, Palepu R. Thermodynamic properties of binary mixtures of butanediols with water. J Solution Chem. 1998;27:17–31.
54. Cipiciani A, Onori G, Savelli G. Structural properties of water-ethanol mixtures: a correlation with the formation of micellar aggregates. Chem Phys Lett. 1988;143:505–9.
55. Tariq M, Forte PAS, Gomes MC, Lopes JC, Rebelo LPN. Densities and refractive indices of imidazolium-and phosphonium-based ionic liquids: effect of temperature, alkyl chain length, and anion. J Chem Thermodyn. 2009;41:790–8.
56. Iglesias-Otero MA, Troncoso J, Carballo E, Romaní L. Density and refractive index in mixtures of ionic liquids and organic solvents: correlations and predictions. J Chem Thermodyn. 2008;2008(40):949–56.
57. Mehra R. Application of refractive index mixing rules in binary systems of hexadecane and heptadecane with n-alkanols at different temperatures. Proc Indian Acad Sci (Chem Sci). 2003;115:147–54.

PRINCIPAL
Govt. Degree College
KARVETINAGAR - 517582
Chittoor Dt. A.P.